Variational Data Assimilation for Determining the Seasonal Net Surface Heat Flux Using a Tropical Pacific Ocean Model

LISAN YU*

Center for Ocean–Atmospheric Prediction Studies and Supercomputer Computations Research Institute, The Florida State University, Tallahassee, Florida

JAMES J. O'BRIEN

Center for Ocean–Atmospheric Prediction Studies, The Florida State University, Tallahassee, Florida

(Manuscript received 15 June 1993, in final form 7 March 1995)

ABSTRACT

The authors present a study for determining the seasonal net surface heat flux over the tropical Pacific Ocean using an adjoint technique. A simple tropical ocean model with thermodynamics is chosen and the seasonal sea surface temperature (SST) observations are assimilated. A least-squares fitting of the model state to data is used. The cost function has a misfit term that measures the difference between the modeled and observed SST and two additional terms that penalize the departure of the estimated parameters from their prior information.

The adjoint method ensures that the flux pattern obtained is consistent with the model's dynamics and thermodynamics and is also in agreement with observations. Comparisons with heat flux atlases of Oberhuber and Fu et al. show that our adjoint calculations have successfully captured the main seasonal signals of the surface heat flux distribution over the tropical Pacific Ocean although, not surprisingly, some differences exist. The differences are examined from both thermodynamic and air–sea interaction viewpoints. Two experiments are conducted to study the effects of the prior information on the optimal solution.

1. Introduction

The variability of surface heat fluxes over tropical oceans is an important question in studies of climate change and air–sea interaction. However, the accurate assessment of surface heat fluxes is greatly limited due to the lack of direct measurements and the insufficient knowledge of air–sea exchange processes. The aerodynamic bulk formulae, the most commonly used means for flux calculations, have shown their inadequacy in providing reliable information about flux distributions (e.g., Blanc 1987). A question to be asked: Is it possible to obtain a better flux field with available observations? In this study we use a novel method by using an ocean model to determine the net heat flux.

Data assimilation has proven to be a powerful tool in extracting the maximum amount of information from observations (Lorenc 1986; Wunsch 1989; Ghil and Malanotte-Rizzoli 1991; Anderson 1991; Bennett 1992). The studies by Lewis and Derber (1985), Le Dimet and Talagrand (1986), Talagrand and Courtier (1987), Derber (1987), Thacker (1988), and Thacker and Long (1988) have made significant contributions to the adjoint approach, which has developed as one of the important strategies in variational data assimilation. An attempt is made here to explore the potential of determining the seasonal surface heat flux distribution by the adjoint method. This problem has been recently studied by several researchers, for example, Tziperman et al. (1992) and Marotzke and Wunsch (1993). However, they have only tackled the problem of the steady-state circulation for the North Atlantic Ocean. In this study the flux field is treated as a time-dependent parameter field, and the annual variability of the net heat flux over the tropical Pacific Ocean is estimated by using a modified reduced-gravity model.

We select the datasets of the climatological sea surface temperature (SST) (Shea et al. 1990) and the climatological wind (Stricherz et al. 1992) because of their fairly good temporal and spatial coverage in the domain of interest. The seasonal variation of the surface heat flux over the tropical Pacific Ocean is determined by assimilating SST observations into a relatively simple reduced-gravity model with thermody-

* Current affiliation: Center for Meteorology and Physical Oceanography, Dept. of Earth, Atmospheric, and Planetary Sciences, Massachusetts Institute of Technology, Cambridge, Massachusetts.

Corresponding author address: Dr. Lisan Yu, Dept. of Earth, Atmos., and Plan. Sci., Massachusetts Institute of Technology, Room 54-1420, Cambridge, MA 02139-4307.
E-mail: lyu@pimms.mit.edu

namics (Cane 1979; Seager et al. 1988). Only the SST observations are involved in the assimilation procedure because the reduced-gravity model used here decouples the thermodynamic equation from the dynamic equation. This reduces the model constraints to the sole SST equation. The momentum equation is driven to the seasonal steady state by the climatological wind. The current field is used, in conjunction with the SST data, to compute the net surface heat flux.

The cost function has a data misfit term that measures the lack of fit between the modeled and observed SST. It also includes the prior information about the estimated parameters. It should be emphasized that the essential part of the cost function is the data misfit term because its gradient is the forcing for the adjoint equation. The prior information is supplemented as penalties and does not alter the nature of the assimilation.

The plan of the paper is as follows. Section 2 discusses the application of the adjoint method to the oceanic model and the formulation of the variational assimilation procedure. In section 3, two experiments are designed to study the effect of the prior information on the estimation of the optimal heat flux distribution. The differences between the flux map from the adjoint procedure and the atlases of Oberhuber (1988, hereafter O88) and Fu et al. (1990, hereafter F90) are analyzed in section 4. A summary and conclusions are included in section 5.

2. Determining the heat flux distribution over the tropical Pacific Ocean by the adjoint technique

a. Methodology

The theoretical foundation of the adjoint technique is the optimal control theory of partial differential equations (Lions 1971). The main issue of the theory is to study the controllability of outputs with respect to inputs. In atmospheric and oceanographic applications, the cost function $J(\mathbf{x}, \mathbf{u})$, which measures the lack of fit between the observation and the model counterpart, is the output. However, the choice of which parameters to be designated as the control vector (input), $\mathbf{u}$, is not unique. Any or all of the parameters, for example, initial conditions, boundary conditions, and any physical or numerical parameters that enter the model formulation, can be taken as control variables. These control values of $\mathbf{u}$ determine the state of the atmosphere and ocean, $\mathbf{x}$, through the model of the system $E(\mathbf{x}, \mathbf{u}) = 0$.

The mathematical formulation for finding the optimal solution can be described as follows:

minimizing the cost function $J(\mathbf{x}, \mathbf{u})$
subject to the equality constraint $E(\mathbf{x}, \mathbf{u}) = 0$.

It states that the optimal state obtained is constrained by conservation laws and/or statistical relationships of real atmospheric or oceanographic fields. It also states that the optimal state should be close to observations within the allowance of the observation accuracy at the given spatial and temporal scales. In other words, this process is able to provide a solution with exact consistency between data and model dynamics.

b. Description of the physical model

Different numerical models are available to study the ocean dynamics and thermodynamics in tropical regions. On the one hand, we have simple models such as the reduced-gravity models (e.g., Bussalacchi and O'Brien 1980; Zebiak and Cane 1987), which have demonstrated the relevance of linear dynamics to the observed annual and interannual variability of tropical oceans. While on the other hand, we might select a general circulation model (GCM) (e.g., Philander and Siegler 1985). Although a GCM is the most complex model existing, it always presents difficulties in the interpretation of its behavior due to the number and the complexity of the processes involved.

The surface heat flux itself is a complicated phenomenon in which radiative, latent, and sensible heat fluxes all contribute to the resulting net flux variations. We hope that the estimated heat flux pattern from the adjoint approach can be explained by intrinsic model physics. For this reason a reduced-gravity model with thermodynamics is chosen that is capable of representing the main mechanisms of dynamic/thermodynamic processes. A suitable model of this type is Cane's reduced-gravity model with a constant-depth surface layer (Cane 1979; Seager et al. 1988).

The model consists of two layers above the thermocline with the same constant density (Fig. 1). The

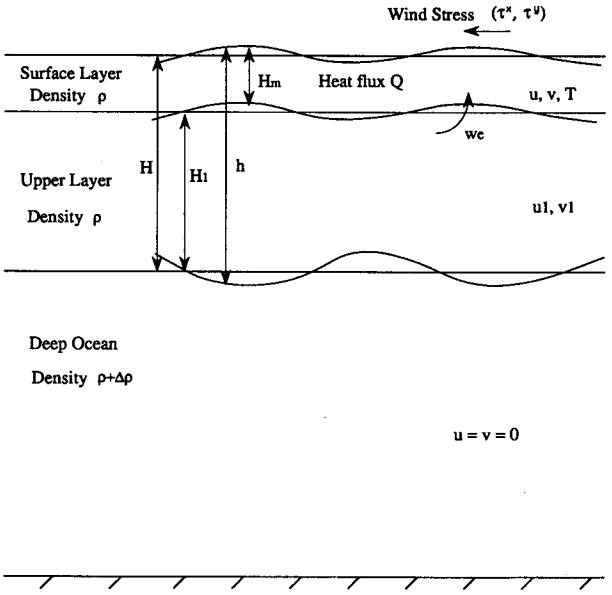

FIG. 1. The vertical structure of the reduced-gravity model with thermodynamics.

ocean below the thermocline, with a higher density, is assumed to be sufficiently deep so that its velocity vanishes. The upper of the two active layers is a fixed-depth surface layer in which the thermodynamics are included. The surface layer communicates with the lower active layer through entrainment/detrainment at their interface and through the frictional horizontal shearing. We assume that there is no density difference across the base of the surface layer; that is, the surface layer is treated as part of the upper layer. Following Seager et al. (1988), the equations for the depth-averaged currents are

$$\frac{\partial u_1}{\partial t} - \beta y v_1 = -g' \frac{\partial h}{\partial x} + \frac{\tau^x}{\rho_0 H} + A\nabla^2 u_1 \quad (2.1a)$$

$$\frac{\partial v_1}{\partial t} + \beta y u_1 = -g' \frac{\partial h}{\partial y} + \frac{\tau^y}{\rho_0 H} + A\nabla^2 v_1 \quad (2.1b)$$

$$\frac{\partial h}{\partial t} + H\left(\frac{\partial u_1}{\partial x} + \frac{\partial v_1}{\partial y}\right) = 0, \quad (2.1c)$$

where (u_1, v_1) are the horizontal velocity components of the depth-averaged currents; h the total layer thickness; H the mean depth of the layer; ρ_0 the density of water; and A the horizontal eddy viscosity coefficient. The wind stress is calculated by the aerodynamic bulk formula

$$(\tau^x, \tau^y) = \rho_a c_D |\mathbf{U}|(U, V),$$

where ρ_a is the density of the air; c_D the wind stress drag coefficient; $\mathbf{U}$ the wind speed vector; and (U, V) the components of the wind velocity.

The equations governing the shear between the surface layer and the lower upper layer are represented by the Ekman dynamics:

$$\gamma_s u_s - \beta y v_s = \frac{\tau^x}{\rho_0 H_m} \quad (2.2a)$$

$$\gamma_s v_s + \beta y u_s = \frac{\tau^y}{\rho_0 H_m}, \quad (2.2b)$$

where (u_s, v_s) are the frictional velocity components, γ_s is the friction coefficient, and H_m the depth of the surface layer over which the stress is applied and is taken to be a constant by assumption.

The entrainment velocity can be calculated from the divergence of the surface layer current field,

$$w_e = H_m\left(\frac{\partial u}{\partial x} + \frac{\partial v}{\partial y}\right). \quad (2.3)$$

The evolution of the SST is governed by the horizontal advection, the vertical entrainment, the surface heating, and the horizontal diffusion. The equation can be expressed as

$$\frac{\partial T}{\partial t} + u\frac{\partial T}{\partial x} + v\frac{\partial T}{\partial y} = \frac{Q}{\rho_0 c_p H_m} + \frac{M(w_e)(T_d - T)}{H_m} + A_T\nabla^2 T, \quad (2.4)$$

where T represents the value of the SST, c_p is the specific heat, and A_T the horizontal diffusion coefficient. The net surface heat flux Q, a function of time and space, involves a field of parameters to be determined by the variational adjoint process. The second term on the right-hand side is the bulk representation of the turbulent heat flux, which occurs when the surface layer entrains water from the layer below. The quantity, T_d, is the subsurface water temperature. Entrainment brings cooler subsurface water to the surface and cools the surface layer. Detrainment, however, warms up the subsurface water but does not directly change the temperature in the surface layer. So the Heaviside step function $M(w_e)$ is introduced, which is defined to be zero for w_e less than zero and equal to w_e for w_e greater than or equal to zero.

As is common in a reduced-gravity model the surface layer pressure gradient is assumed to be a function of the thermocline depth alone. This implies that the effect of the SST change on the pressure gradient is negligible—a condition that may not hold universally. Therefore, this assumption cannot be rigorously justified. Fortunately, by assuming this the model physics are greatly simplified since the dynamics and the thermodynamics become decoupled. The dynamical fields [Eqs. (2.1)–(2.3)] have a significant influence on the SST evolution [Eq. (2.4)] through the advection process but they will not be affected by any SST change. In other words, changes in the SST due to changes of the surface heat flux have no effect on the dynamical fields. This further simplifies our parameter estimation problem because the constraints of the system reduce to a single SST equation.

c. *The formulation of the cost function*

The cost function defines the objective of the minimization and is the core part of the adjoint assimilation. Considering the linear dynamics of our model, we choose a least-squares fitting for the cost function corresponding to a L_2 Euclidean norm. The cost function is then defined as

$$J(T, Q, T_0) = \frac{1}{2}\sum_{i,j,n}(T - \hat{T})^{\mathrm{T}}\mathbf{K}_T(T - \hat{T}) + \frac{1}{2}\sum_{i,j,n}(Q - \tilde{Q})^{\mathrm{T}}\mathbf{K}_Q(Q - \tilde{Q}) + \frac{1}{2}\sum_{i,j}(T_0 - \tilde{T}_0)^{\mathrm{T}}\mathbf{K}_{T_0}(T_0 - \tilde{T}_0), \quad (2.5)$$

where the superscript T denotes transpose, the caret the available climatological data, and the tilde the prior in-

formation. The summation is spanned over the observational space–time domain. The $\mathbf{K}$ are weighting matrices and theoretically should be the inverse of the observation error covariance matrices. By assuming, for simplicity, that errors in the data are uncorrelated and have equal variance, these weighting matrices can be written as

$$\mathbf{K}_l = \sigma_l^{-2}\mathbf{I}, \tag{2.6}$$

where l represents T, Q, or T_0, and σ^2 is a positive scalar whose magnitude is given in the next section associated with the experiment design.

The minimization problem will not be altered if we scale (2.5) with K_T and search the optimal value of the following cost function J (the prime is neglected for simplicity):

$$\begin{aligned} J(T, Q, T_0) = &\frac{1}{2}\sum_{i,j,n}(T - \hat{T})^{\mathrm{T}}(T - \hat{T}) \\ &+ \frac{1}{2}\beta_1 \sum_{i,j,n}(Q - \tilde{Q})^{\mathrm{T}}(Q - \tilde{Q}) \\ &+ \frac{1}{2}\beta_2 \sum_{i,j}(T_0 - \tilde{T}_0)^{\mathrm{T}}(T_0 - \tilde{T}_0) \\ &\equiv J_T + \beta_1 J_Q + \beta_2 J_{T_0}, \end{aligned} \tag{2.7}$$

where $\beta_1 = \sigma_T^2/\sigma_Q^2$ and $\beta_2 = \sigma_T^2/\sigma_{T_0}^2$, representing the relative weights associated with each penalty.

There are three terms in the cost formulation (2.7). The first term, named as J_T, represents the misfits between the modeled SST and the observed SST; the second one, J_Q, measures the departure of the estimated net surface heat flux field from some guess flux field; and the last one, J_{T_0}, is added to control the initial condition estimation. The last two terms represent the prior information whose form quantifies our expectation about the character of the solution.

A unique solution of (2.7) exists when two conditions are satisfied. First, the inverse problem of (2.7) is well determined. Theoretically this can occur if the number of control parameters is less than the number of independent observations. The second condition is that the cost function of (2.7) should be convex in the parameter space. This requirement is satisfied only if the Hessian matrix of the second derivatives of the cost function is positive definite. The Hessian of cost part J_T of (2.7) is

$$\frac{\partial^2 J}{\partial x^2} = \sum_{i,j,n}\left[\left(\frac{\partial T}{\partial x}\right)^{\mathrm{T}}\left(\frac{\partial T}{\partial x}\right) + (T - \hat{T})^{\mathrm{T}}\frac{\partial^2 T}{\partial x^2}\right], \tag{2.8}$$

where x represents the independent variables Q or T_0. The first term on the right-hand side is positive semidefinite and the second term could be negative—which means their sum is not positive definite by default. The minimization of the cost part J_T alone could not guarantee a unique solution. However, the contribution of the prior information J_Q and J_{T_0} to the Hessian of (2.7) is positive (quantified by K_Q and K_{T_0}). The inclusion of the prior information can, in general, increase the probability of the positive definiteness of (2.8) and enhance the convexity of the cost function of (2.7).

The initial condition is enforced here because of its importance in obtaining appropriate values of model controls (Yu and O'Brien 1991, 1992). The model equation (2.4) is a linear partial differential equation (PDE) with nonconstant coefficients. The heat flux plays the role of external forcing. The solution of the PDE is determined by the initial condition, the boundary condition, and the forcing. Regardless of the lateral boundary condition, which has shown the negligible effect on the solution in this case, the behavior of the equation (2.4) is controlled by the initial SST state and the heat flux forcing field. Therefore, in addition to the heat flux field, a model-balanced initial condition is another important factor in determining the solution.

d. The variational adjoint procedure

The SST equation (2.4) can be enforced as a strong constraint by introducing a set of Lagrange multipliers λ_T. This leads to the formation of the following augmented Lagrangian function (Navon and De Villiers 1983):

$$\begin{aligned} L(T, Q, T_0, \lambda_T) = &J(T, Q, T_0) \\ &+ \sum_{i,j,n}\lambda_T\left\{\frac{\partial T}{\partial t} + u\frac{\partial T}{\partial x} + v\frac{\partial T}{\partial y} - \frac{Q}{\rho_0 c_p H_m}\right. \\ &\left. - \frac{M(w_e)(T_d - T)}{H_m} - A_T\nabla^2 T\right\}. \end{aligned} \tag{2.9}$$

By doing so, the constrained optimization problem is replaced by a series of unconstrained problems with respect to variables T, Q, T_0, and λ_T. The difficulty of finding the minimum of the cost function while satisfying the SST equation is transformed into the problem of finding the stationary point of the Lagrangian function. Note that not all variables are independent. The variations of the controls Q and T_0 are determined by the optimization process and the subsequent variations of the dependent variable T are given by the SST equation.

The condition of the stationary point of the Lagrangian function $L(T, Q, T_0, \lambda_T)$ requires that the first variation of $L(T, Q, T_0, \lambda_T)$ with respect to all the variables vanish. This results in the following set of equations:

$$\frac{\partial L(T, Q, T_0, \lambda_T)}{\partial \lambda_T} = 0 \tag{2.10}$$

$$\frac{\partial L(T, Q, T_0, \lambda_T)}{\partial T} = 0 \tag{2.11}$$

$$\frac{\partial L(T, Q, T_0, \lambda_T)}{\partial Q} = 0 \tag{2.12}$$

$$\frac{\partial L(T, Q, T_0, \lambda_T)}{\partial T_0} = 0. \quad (2.13)$$

Equation (2.10) recovers the original SST equation. Combining the continuity equation (2.3) with (2.4), one can write the SST equation as

$$\frac{\partial T}{\partial t} + \frac{\partial (Tu)}{\partial x} + \frac{\partial (Tv)}{\partial y} - A_T \nabla^2 T - \left\{ \frac{M(w_e)(T_d - T)}{H_m} - \frac{w_e T}{H_m} \right\} = \frac{Q}{\rho_0 c_p H_m}. \quad (2.14)$$

Equation (2.11) is the adjoint equation, whose explicit form is

$$\frac{\partial \lambda_T}{\partial t} + \frac{\partial (\lambda_T u)}{\partial x} + \frac{\partial (\lambda_T v)}{\partial y} + A_T \nabla^2 \lambda_T - \frac{\lambda_T M(w_e)}{H_m} = (T - \hat{T}). \quad (2.15)$$

Comparing Eq. (2.14) with Eq. (2.15), one can find that the adjoint equation has a similar form to the SST equation except for two prominent features. The driving factor in the adjoint equation is the gradient of the data misfit in contrast to the surface heat flux in the SST equation. In addition, the diffusion term in the adjoint equation has an opposite sign to that in the SST equation. This requires that the integration of the adjoint equation should be backward in time in order to satisfy the stability condition of a well-posed problem. Therefore, the Lagrange multiplier provides the information about how different the data and the model counterparts are. This information is transmitted back to the initial time of the assimilation cycle to influence the reconstruction of the model state.

Equation (2.12) is satisfied only when the optimal solution is found. During the iterative procedure, the left-hand side of (2.12) provides the gradient information of the cost function J with respect to the control variables Q; that is,

$$g_Q \equiv \nabla_Q J = \beta_1 (Q - \tilde{Q}) - \frac{\lambda_T}{\rho_0 c_p H_m}. \quad (2.16)$$

This gradient information is used with some descent algorithm (e.g., conjugate gradient method) to form a new search direction d_Q. The update of the control Q is based on the following relation:

$$Q^{\text{new}} = Q^{\text{old}} + s d_Q, \quad (2.17)$$

where s, a scalar, is the step size that determines how far the search should be along the direction d_Q. The initial condition is adjusted in a similar way; that is,

$$T_0^{\text{new}} = T_0^{\text{old}} + s d_{T_0}, \quad (2.18)$$

where the construction of the search direction d_{T_0} uses the gradient information

$$g_{T_0} \equiv \nabla_{T_0} J = \beta_2 (T_0 - \tilde{T}_0) - \lambda_{T|t=0}. \quad (2.19)$$

The variational adjoint procedure starts from best guess values of the controls Q and T_0 and uses them to integrate the SST equation (2.14). The whole time history of the SST evolution is saved to compute the gradient of the data misfit. The adjoint equation (2.15) is integrated backward in time using the knowledge of the model − data difference. The cost gradients with respect to Q and T_0 [relations (2.16) and (2.19)] are computed from the value of the Lagrange multiplier and are used to construct the search directions d_Q and d_{T_0}. At the end of each iteration, the controls are corrected by using (2.17) and (2.18). If the stopping criteria are reached, the solution at the present iteration is regarded as the optimal solution and the procedure is terminated. Otherwise, the procedure continues and the SST equation is stepped forward with the new estimates of the controls. Note that in the integration of both the SST equation and the adjoint equation, one needs to know the dynamical fields such as the currents and thermocline depth. So the trajectory of the dynamical model [(2.1)−(2.3)] must be computed in advance in order to perform the minimization procedure.

e. Numerical models

The dynamical model [Eqs. (2.1)−(2.3)] is governed by wave dynamics. For the chosen model domain that extends from 25°S to 25°N in latitude and from 120°E to 70°W in longitude, all possible equatorially trapped waves, for example, Kelvin, Rossby, Yanai, and gravity waves, can be excited by the applied wind forcing (Moore and Philander 1978). The temporal and spatial resolutions of the numerical model have to be appropriately chosen in order to resolve all the possible waves and also to make the model integration numerically stable.

We choose the spatial interval for the dynamical model to be $\Delta x = \Delta y = 0.5°$ and the time step to be $\Delta t = 15$ min. The model [(2.1)−(2.3)] is driven by the FSU (Florida State University) climatological monthly mean winds (Stricherz et al. 1992). The data are projected into each time step by a linear interpolation and into each grid point by a cubic-spline interpolation. The values of numerical parameters used in the model integration are listed in Table 1. It takes about 12 years for the model to reach a periodic constant seasonal cycle; at that time the main seasonal variability of dynamical fields has been successfully captured. The currents and the upper layer thickness of the 16th year are saved to be used in the minimization.

The horizontal resolution for the SST equation and its adjoint is chosen to be $\Delta x = \Delta y = 2°$. A longer time step, $\Delta t = 6$ h, is used and the total integration time is 360 days. The datasets of the climatological monthly mean SST from Shea et al. (1990) (Figs. 2a–d) are chosen for the assimilation. The adjoint procedure performs, in each iteration, one forward SST model integration and one backward adjoint integration

TABLE 1. The values of the model parameter used in the model integration.

Parameter	Value	Remarks
H	150 m	Mean depth of upper layer
H_m	50 m	Depth of the constant surface layer
g'	3.7×10^{-2}	Reduced gravity
c_D	1.5×10^{-3}	Wind stress drag coefficient
ρ_a	1.2 kg m^{-3}	Density of air
ρ_0	1025 kg m^{-3}	Density of seawater
R	6.3784×10^6 m	Radius of earth
Ω	0.729×10^{-4} sec^{-1}	Angular rotation rate of the earth
c_p	3.994×10^3 J (kg °C)$^{-1}$	Specific heat
A	750 m^2 sec^{-1}	Coefficient of horizontal viscosity
A_T	2000 m^2 sec^{-1}	Coefficient of horizontal thermal diffusion
r_s	0.5 (day)$^{-1}$	Dissipation coefficient

in order to compute the gradient of the cost function. The descent algorithm of CONMIN routine (Shanno and Phua 1980; Navon and Legler 1987) carries out the task of searching the optimal cost value. Several such iterations are performed to obtain the minimum of the cost function.

The model is discretized on the Arakawa C-grid, and the model northern and southern boundaries are open. The radiation boundary condition described by Camerlengo and O'Brien (1980) is imposed to compute model variables along these boundaries. The coastal effect at the eastern and western sides of the basin is simulated. The no-normal flow and no-slip conditions are applied at these solid boundaries. The time integration uses a leapfrog scheme, with a forward scheme every 99th time step to eliminate the computational mode. A Dufort–Frankel scheme is employed for the diffusion term (O'Brien 1986).

3. Experiment design

a. Experiment 1

In this experiment we adopt an approach originated from the statistical theory (Neuman 1973) in which the misfit is based on the statistics of observations and the penalty criterion is based on the statistics of prior parameter estimates. The method recognizes that the prior statistics either determined from the observations or based upon the theoretical considerations will seldom be known with sufficient accuracy. For this reason the relative weights of the misfit and penalty terms, that is, β_1 and β_2 in (2.7), do not need to be specified exactly but are determined by the residual analysis method during the procedure. By doing so, the problem of estimating the heat flux and initial SST can be posed as the problem of finding a particular vector Q and T_0, which minimize the cost function (2.7) under a given β. That is to say, the cost function (2.7) is minimized for a sequence of β values in addition to a sequence of Q and T_0 values.

How do we select the optimum value of β? The basic assumption is that the optimum value of β is the value that leads to the minimum variance of the estimation error $e_Q = Q_e - Q_{\text{true}}$, where Q_e is the estimate of Q_{true} (Neuman 1980). This implies that, when β is at its optimum value, the statistical properties of the computed residuals is closest to those predicted by theory. Hence, we should be able to identify the optimum value of β by analyzing how the properties of the residuals change with β. This is the theoretical basis of the residual analysis (Draper and Smith 1981).

Neuman and Yakowitz (1979) and Neuman (1980) have listed several statistical criteria to select the optimum value of β. In addition, a scheme based on the method of stagewise optimization (Bard 1974) was proposed by Carrera and Neuman (1986a,b), which we found very appealing in practice and hence adopted in our study. By incorporating their scheme, the iterative procedure is performed as follows.

(i) starting from a good initial guess for the controls (T_0 and Q) and for the β (note that the choice of initial β can be arbitrary. We choose $\beta_1 = \beta_2 = 1$).

(ii) integrating the SST equation forward.

(iii) calculating the cost components J_T, J_Q, and J_{T_0} and setting the new value of β according to

$$\beta_1 = \tilde{\sigma}_T^2/\tilde{\sigma}_Q^2 \quad \text{and} \quad \beta_2 = \tilde{\sigma}_T^2/\tilde{\sigma}_{T_0}^2, \qquad (3.1)$$

where $\tilde{\sigma}_T^2 = J_T/N_T$, $\tilde{\sigma}_Q^2 = J_Q/N_Q$ and $\tilde{\sigma}_{T_0}^2 = J_{T_0}/N_{T_0}$. The integer N_l is the number of l-type parameters for which observed/prior data are available.

(iv) integrating the adjoint equation backward.

(v) performing the CONMIN descent algorithm to search a new estimate for the controls Q and T_0 to minimize the cost function of (2).

(vi) repeating the steps (ii)–(v) until the convergence criteria are satisfied.

In the equatorial region the two major components in the SST equation are the surface heat flux and the upwelling. By balancing there two terms we can deduce the initial Q field. The initial SST field is taken from the spinup run. At the kth iteration (where k is the iteration number), the prior information $\tilde{Q}_k$ is given to the value of Q_{k-1}. (The same holds for $\tilde{T}_0$; that is, $\tilde{T}_{0_k} = T_{0_{k-1}}$.) Mathematically, the penalty terms in the present form behave somewhat like the multiplier penalty (Fletcher 1987). The degree of the penalty is represented by the value of β and the origin of the penalty is given by $\tilde{Q}$. The actual usefulness of these terms is that it can enhance the convexity of the cost function J with the benefits of increasing the probability of the unique solution and accelerating the convergence of the minimization algorithm (Yu 1992).

The evolution of the cost function and the norm of its gradient during the minimization is shown in Fig. 3.

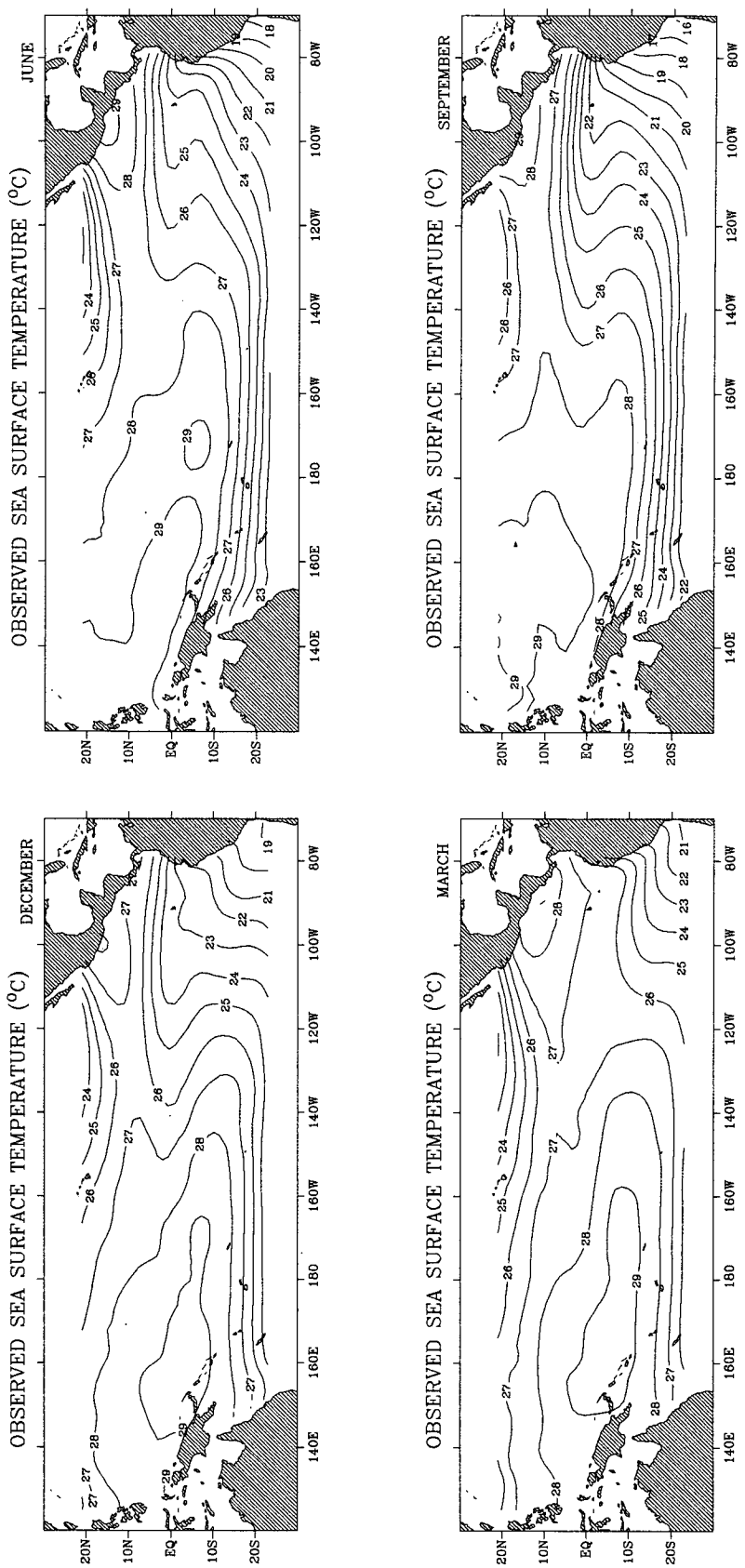

FIG. 2. The observed sea surface temperature (SST) in (a) December, (b) March, (c) June, and (d) September (contour interval is 1°C).

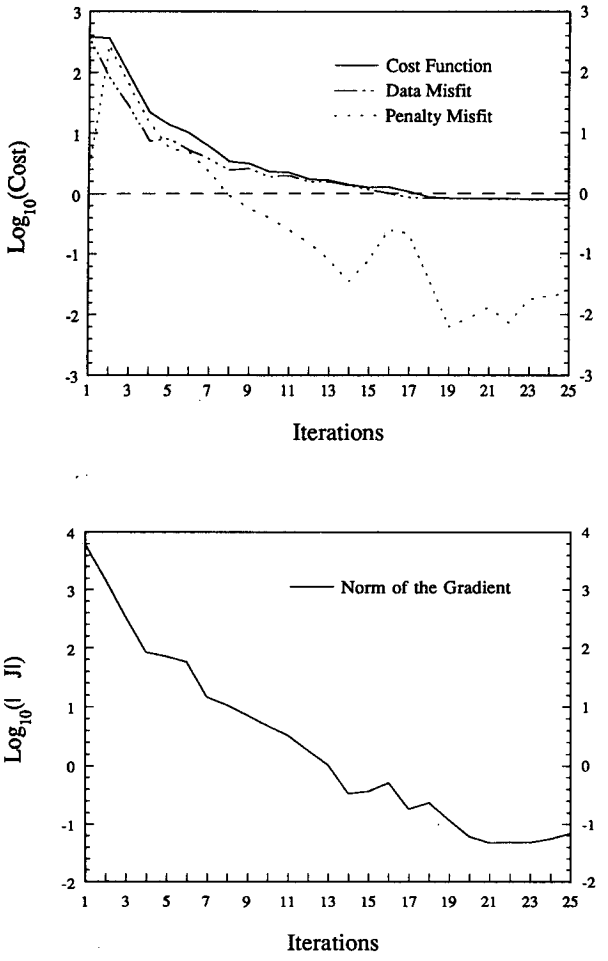

FIG. 3. The evolution of (a) the cost function (the zero line represents the standard deviation of the data misfit) and (b) the norm of the gradient during the minimization (experiment 1).

The norm of the gradient decreases rapidly during the first 8 iterations. Correspondingly, the value of the cost function has a great reduction in these 8 iterations. The iterative process is terminated after 25 iterations since the cost function does not have any tendency for further improvement. Figure 3 also displays that the penalty terms J_Q and J_{T_0} have a bigger impact on the procedure at the initial stage and oscillate around $O(10^{-2})$ when the optimal solution is approached. Nevertheless, as long as these two terms remain different from zero, they are constraining the solution.

How can we assess the reliability and precision of the estimate? This issue can be studied by analyzing the estimation error through the two commonly used statistical tools, the mean and the variance. For simplicity let us take an example of the analysis of the estimation error e_Q. The estimation error for Q, under a given β, is

$$e_Q = Q_e - Q_{\text{true}}. \tag{3.2}$$

Under the assumption that the model is exactly valid (the foundation of the adjoint approach), the error e_Q must be related to the error in the data. Therefore, we also want to study the first two moments of the estimation error e_T, which is

$$e_T = T_e - T_{\text{true}}, \tag{3.3}$$

where Q_e and T_e are the least-squares estimates for the "true" Q_{true} and T_{true}.

The SST equation can be written as

$$AT = Q + B, \tag{3.4}$$

where $A = \rho_0 c_p H_m\{\partial/\partial t + \partial(\cdot u)/\partial x + \partial(\cdot v)/\partial y + (M(w_e)/H_m - w_e/H_m) - A_T\nabla^2\}$ and $B = \rho_0 c_p M(w_e) T_d$. Left multiplying the above equation with A^{-1} leads to the relationship

$$T = F(Q) = A^{-1}Q + A^{-1}B. \tag{3.5}$$

Solution of the nonlinear system (3.5) can generally be sought through either of two approaches (Cooley 1977, 1982; Neuman and Yakowitz 1979; Draper and Smith 1982): One method is based on various modifications to the method of steepest descent. The other utilizes Taylor series expansions to linearize the problem. We opted to use the second approach adjoined with the linear regression theory to perform the error analysis.

The following models can be assumed in the analysis.

The measurement model:

$$\hat{T} = T_{\text{true}} + \epsilon, \tag{3.6}$$

where ϵ is a noise vector whose statistical properties are

$$E(\epsilon) = 0 \tag{3.7}$$

$$C(\epsilon) = \sigma_T^2 I. \tag{3.8}$$

The estimation model:

$$Q_e = Q_{\text{true}} + \vartheta, \tag{3.9}$$

where ϑ is a noise vector that uncorrelated with ϵ and whose mean and variance are given by

$$E(\vartheta) = 0 \tag{3.10}$$

$$C(\vartheta) = \sigma_Q^2 I. \tag{3.11}$$

By assuming that the data error ϵ is very small (consequently e_Q is small), we can approximate $F(Q)$ in (3.5) by the linear part of Taylor series expansion; that is,

$$F(Q) \approx F(Q_e) + G(Q - Q_e), \tag{3.12}$$

where $G = (\partial F(Q)/\partial Q)|_{Q=Q_e} = (\partial T/\partial Q)|_{Q=Q_e}$, which is a sensitivity estimator. If we substitute the system model equation (3.12) into the measurement model (3.6), a new expression is obtained:

$$\hat{T} = T_{\text{true}} + \epsilon = F(Q_{\text{true}}) + \epsilon = F(Q_e) + G(Q_{\text{true}} - Q_e) + \epsilon. \quad (3.13)$$

Together with (3.7)–(3.11), we can formulate a linear regression model

$$Y \approx MQ_{\text{true}} + \eta, \quad (3.14)$$

where

$$Y = \begin{bmatrix} \hat{T} - F(Q_e) + GQ_e \\ Q_e \end{bmatrix} \quad M = \begin{bmatrix} G \\ I \end{bmatrix} \quad \eta = \begin{bmatrix} \epsilon \\ \vartheta \end{bmatrix}.$$

The first two moments of η are

$$E(\eta) = 0 \quad (3.15)$$

$$C(\eta) \equiv E(\eta\eta^{\mathrm{T}}) = \sigma_T^2 \begin{bmatrix} I & 0 \\ 0 & \beta_1^{-1} I \end{bmatrix} \Leftarrow \left(\text{by using } \beta_1 = \frac{\sigma_T^2}{\sigma_Q^2} \right). \quad (3.16)$$

If we denote Q_l to be the estimate of Q_{true} corresponding to the linearized model (3.14) and minimize the cost function:

$$J_l(Q_l) = \frac{1}{2}(Y - MQ_l)^{\mathrm{T}}[C(\eta)]^{-1}(Y - MQ_l), \quad (3.17)$$

then according to the multiple linear regression formula (Bard 1974), the best least-squares estimate, Q_l^*, must satisfy

$$Q_l^* = (M^{\mathrm{T}}[C(\eta)]^{-1}M)^{-1}M^{\mathrm{T}}[C(\eta)]^{-1}Y. \quad (3.18)$$

Suppose that Q_l^* is very close to Q_e, the estimation error in (3.2) can be expressed as

$$e_Q \approx Q_l^* - Q_{\text{true}} = (M^{\mathrm{T}}[C(\eta)]^{-1}M)^{-1}M^{T}[C(\eta)]^{-1}(Y - MQ_{\text{true}}) \equiv P^{\mathrm{T}}(Y - MQ_{\text{true}}). \quad (3.19)$$

By our assumption, $E(Y) = MQ_{\text{true}}$ and $C(Y - MQ_{\text{true}}) = C(\eta)$, we obtain

$$E(e_Q) = 0 \quad (3.20)$$

$$C(e_Q) = P^{\mathrm{T}}C(Y - MQ_{\text{true}})P = (M^{\mathrm{T}}[C(\eta)]^{-1}M)^{-1} = \sigma_T^2(G^{\mathrm{T}}G + \beta_1 I)^{-1}. \quad (3.21)$$

The estimation error in (3.3) can also be derived:

$$e_T = T_e - T_{\text{true}} = T_e - (\hat{T} - \epsilon) = T_e - F(T_e) + Ge_Q = Ge_Q. \quad (3.22)$$

By virtue of (3.20) and (3.21), we have

$$E(e_T) = 0 \quad (3.23)$$

$$C(e_T) = GC(e_Q)G^{\mathrm{T}} = \sigma_T^2 G(G^{\mathrm{T}}G + \beta_1 I)^{-1}G^{\mathrm{T}}. \quad (3.24)$$

The statistical properties (3.21) and (3.24) show that the variances of e_T and e_Q are bounded as long as β_1 is sufficiently large. In other words, β_1 has the stabilizing effect in case the sensitivity estimator G is ill conditioned. However, the computation of these covariance matrices is extremely expensive due to the size of the problem. A residual analysis is then performed to examine whether the results are consistent with the a priori assumptions.

At the optimal solution the data misfit value should be at the noise level of the SST data. The misfit J_T of (2.7) starts from $7.2 \times 10^2\sigma_T^2$ and reaches $0.8\sigma_T^2$ when the procedure is terminated. Prior error analysis indicates that the standard derivation of the SST observation error, σ_T, is around 1°C. This results in the misfit value of 0.8 at the optimal solution. Considering that the land points account for 15% of total grid points, the cost function evaluated is approximately at the noise level, and therefore the solution is statistically acceptable.

The resulting optimal net downward surface heat flux distribution is shown in Figs. 4a–d. The pattern displays a strong seasonal cycle. During northern wintertime (Fig. 4a), the zero net heat flux line is located at about 8°N across the whole basin. Heat loss occurs to the north of the zero line, while heat gain occurs to the south of the zero line. The maximum heat loss, over 120 W m^{-2}, happens in the northwestern part of the Pacific over the Kuroshio region. The maximum heat gain area is located in the eastern Pacific near the coast of South America, the area associated with the cold tongue. As spring approaches (Fig. 4b), the pattern begins to change: The heat loss in the northern ocean decreases. Meanwhile, the southern ocean experiences the heat release. The maximum heat gain center in the eastern Pacific expands westward along the equator.

The pattern of the net downward heat flux in June (Fig. 4c) is opposite to that in December. The obvious change occurs near the coast of South America where a considerable amount of heat loss appears. In general, the northern ocean receives the heat and the southern ocean loses the heat. The strength of the heat gain center along the equator decreases to 80 W m^{-2} and moves farther westward. In September when boreal autumn comes, the heat loss/gain activities are weak away from the equator (latitudes poleward of 8°) except over the Kuroshio region where the heat loss is greater than 60 W m^{-2} (Fig. 4d).

The spatial structure of the modeled SST field (Figs. 5a–d) resembles well that of the observed SST field (Figs. 2a–d) except in the equatorial cold tongue region. The misfit maps between these two fields (Figs. 6a–d) also illustrate that the value of the misfit is generally small over the whole basin but is larger (>1°C) in the regions associated with the cold tongue and the Kuroshio.

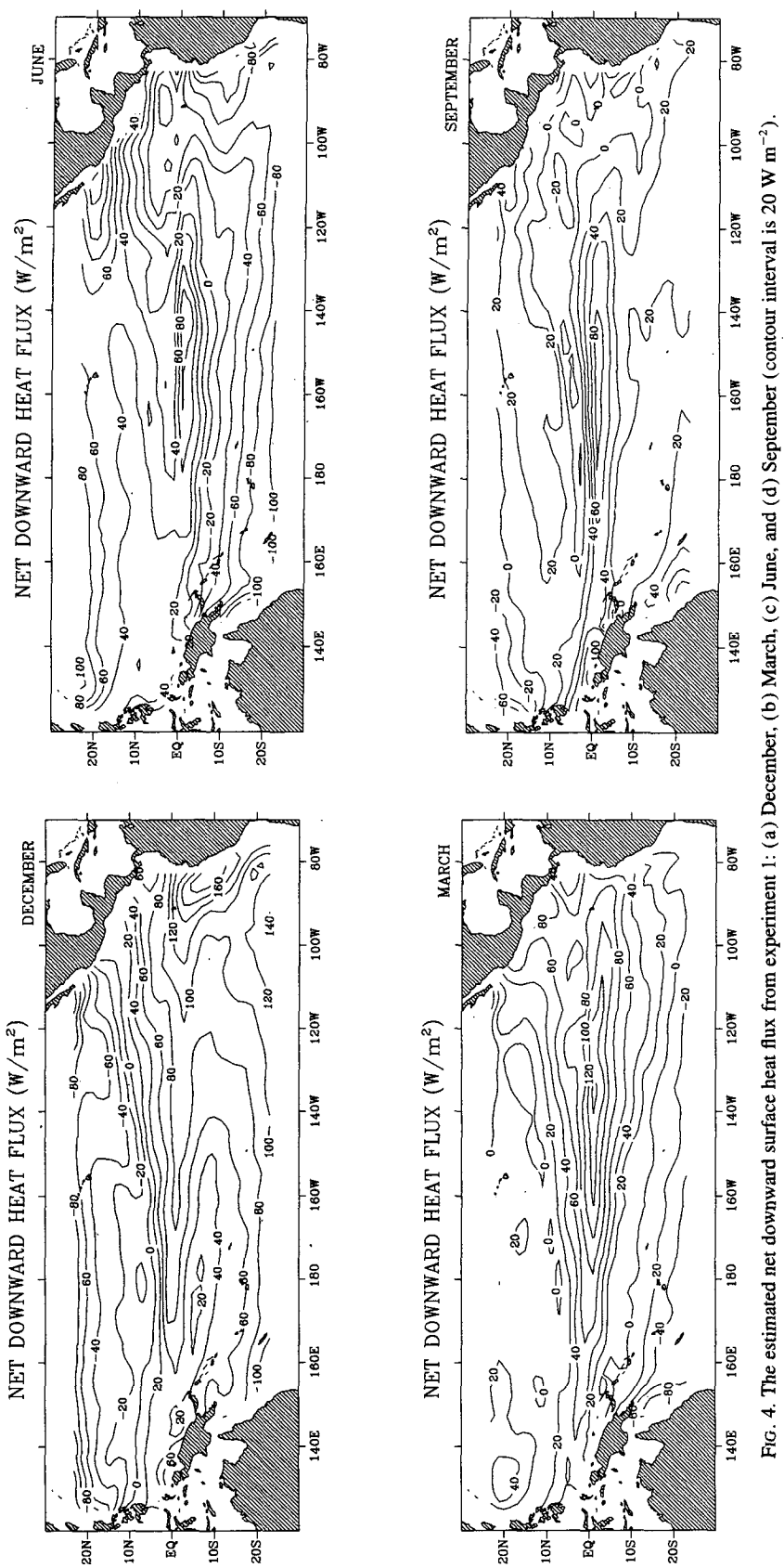

FIG. 4. The estimated net downward surface heat flux from experiment 1: (a) December, (b) March, (c) June, and (d) September (contour interval is 20 W m^{-2}).

b. Experiment 2

Most adjoint approaches used in the oceanographic literature have so far adopted the same ideology; that is, the weighting in (2.7) is prespecified and the prior information is taken to be the observed data. The scheme used in experiment 1 differs from those conventional approaches in two aspects: First, this scheme takes into consideration the uncertainty in the weighting and requires the procedure to determine the weights during the optimization. Second, this scheme asks the prior information u_{prior} to represent the smoothness character of the solution and hence the value of u_{prior} is given to be the value of Q calculated at the previous iteration. These two properties reveal that the approach adopted in experiment 1 emphasizes more the statistical properties of the solution while the conventional approaches put more focus on the use of the available datasets.

Experiment 2 is designed to imitate the conventional approach. The Oberhuber climatological heat flux data (hereafter O88, Figs. 7a–d) are used as the prior information $\tilde{Q}$. At each iteration, the newly computed flux field parameters are compared with the fixed flux data. The adjoint procedure searches for the solution that minimizes the SST misfit and the misfit between the estimated flux and the O88. The initial SST state is adjusted at every iteration but is not penalized in the cost function. The first guess for the heat flux is the same as that in experiment 1.

The standard deviations are estimated as $\sigma_T = 1°C$ for the SST and $\sigma_Q = 50$ W m^{-2} (Weare et al. 1981) for the heat flux. These errors take into account measurement and sampling errors as well as errors due to the missing physics in the model and errors introduced by the interpolation schemed used for processing the data. Precise error estimates for the climatological data are difficult to obtain; the values provided above are considered to be accurate within an order of magnitude.

The resulting heat flux estimation is shown in Figs. 8a–d. Comparing with the flux pattern from experiment 1 (Figs. 4a–d), one finds that the spatial structures from these two experiments are remarkably similar but the strength of the flux field obtained from the present experiment is weaker. The spatial structure of the modeled SST (Figs. 9a–d) is also similar to that of experiment 1 (Figs. 5a–d). However the misfit plots (Figs. 10a–d) show that the SST data misfit value is in general larger than that of experiment 1.

The construction of the adjoint procedure (section 2d) unveils that the SST misfit J_T is the core part of the inverse problem—the gradient of J_T brings the physical information from the SST equation (the constraint of the inverse system) to the adjoint equation and contributes to the search for the better value of parameter Q. It is not surprising to observe that the structures from both experiments look similar. The weaker heat flux estimated from the present experiment is also expected. As is pointed out in section 2c the term J_Q functions as a penalty. It penalizes the departure of the estimated flux field Q from the prior information $\tilde{Q}$. If the optimally determined heat flux field is very different from $\tilde{Q}$, as is the case here, the adjoint procedure tends to give a weaker Q in order to maintain less inconsistency between the simulated SST and the observed SST. The optimal solution obtained is actually a compromise between the data cost J_T and the flux penalty J_Q.

The iterative procedure is terminated after 28 iterations (Fig. 11). At that time the cost values are 1.80 for the data misfit term and 2.02 for the penalty misfit term. As we know when the optimal solution is reached, the misfit should be at the noise level and the global rms of each misfit term should be of order unity to be consistent with their prior estimated standard deviations. Apparently the optimal cost from this run is larger than what it should be. Examining the SST misfit pattern (Figs. 10a–d) one can observe a SST discrepancy greater than 2°C shown in Figs. 10b–c. The heat flux misfit pattern (Figs. 12a–d) shows that the maximum heat flux discrepancy is around 140 W m^{-2} and the average misfit is larger than the prior estimate of 50 W m^{-2}. Judging from prior error estimation, the optimal solution is not consistent with the Oberhuber's heat flux atlas.

It should be addressed that the expectations of the solution in these two experiments are incommensurate: one employs the statistical criteria to the solution (experiment 1) and the other explores the solution under the constraint of the existing flux atlases (experiment 2). Therefore, the two solutions are fundamentally not comparable. There is no unique criterion to make a judgement for which solution is better. However, one should notice that the results from experiment 1 are dependent upon the ad hoc prior error estimate. Whether the solution is unique when different atlases are used is yet unknown and subject to future study.

In the following section we are going to conduct the theoretical analysis to the estimated heat flux pattern and to compare it with the existing flux atlases. The results from experiment 1 are chosen solely because those results are obtained by assimilating the SST data only, independent of any of the flux atlases.

4. Results analysis

a. Comparisons with the existing heat flux atlases

Although many versions of climatological fluxes are available, a considerable amount of uncertainty exists among these atlases due to the implementation of different heat flux parameterization schemes. There is no standard version in existence allowing us to make a good judgement about our calculations. Hence, the two atlases chosen, O88 and F90, serve only to illustrate the general features of the heat flux seasonality.

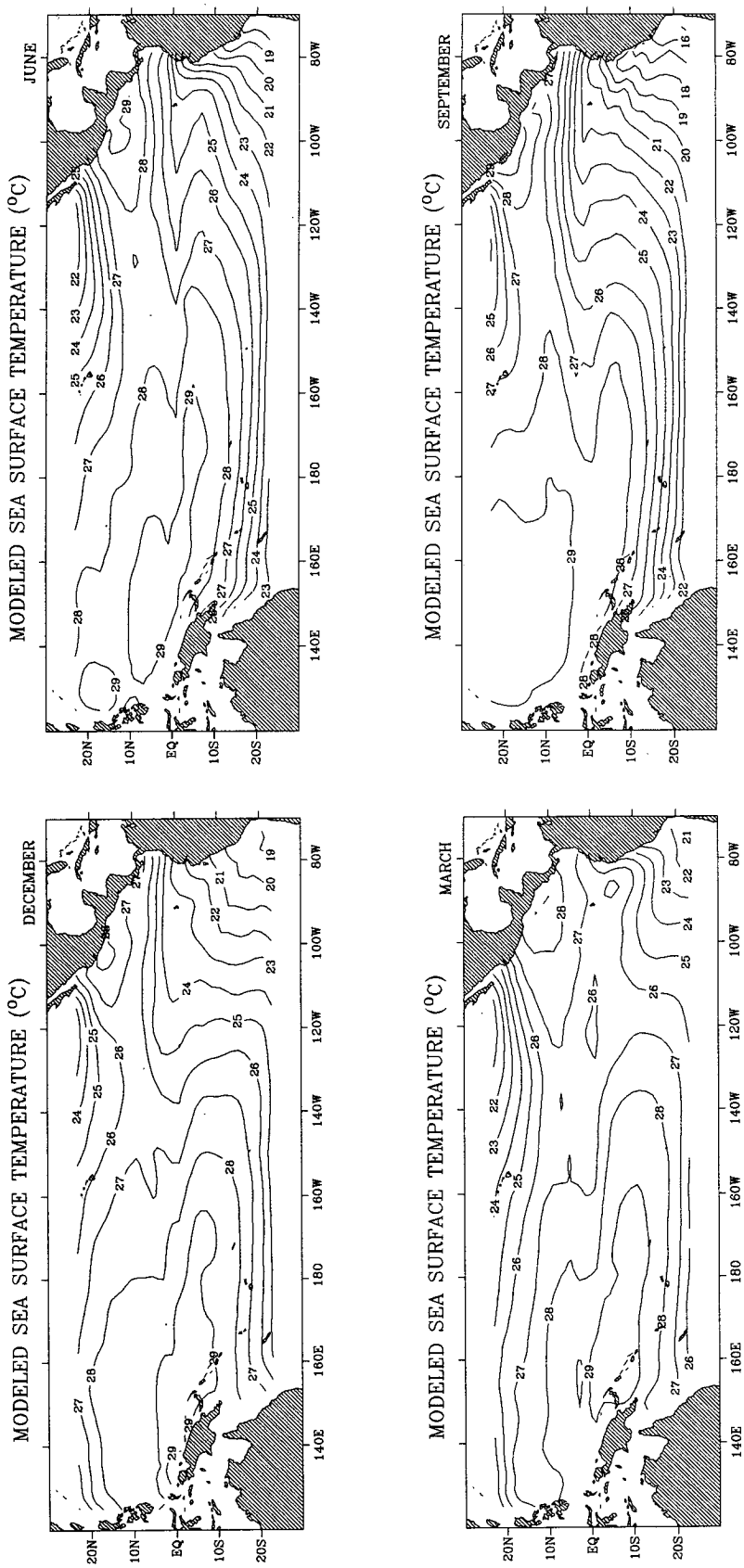

FIG. 5. The modeled SST (experiment 1) in (a) December, (b) March, (c) June, and (d) September (contour interval is 1°C).

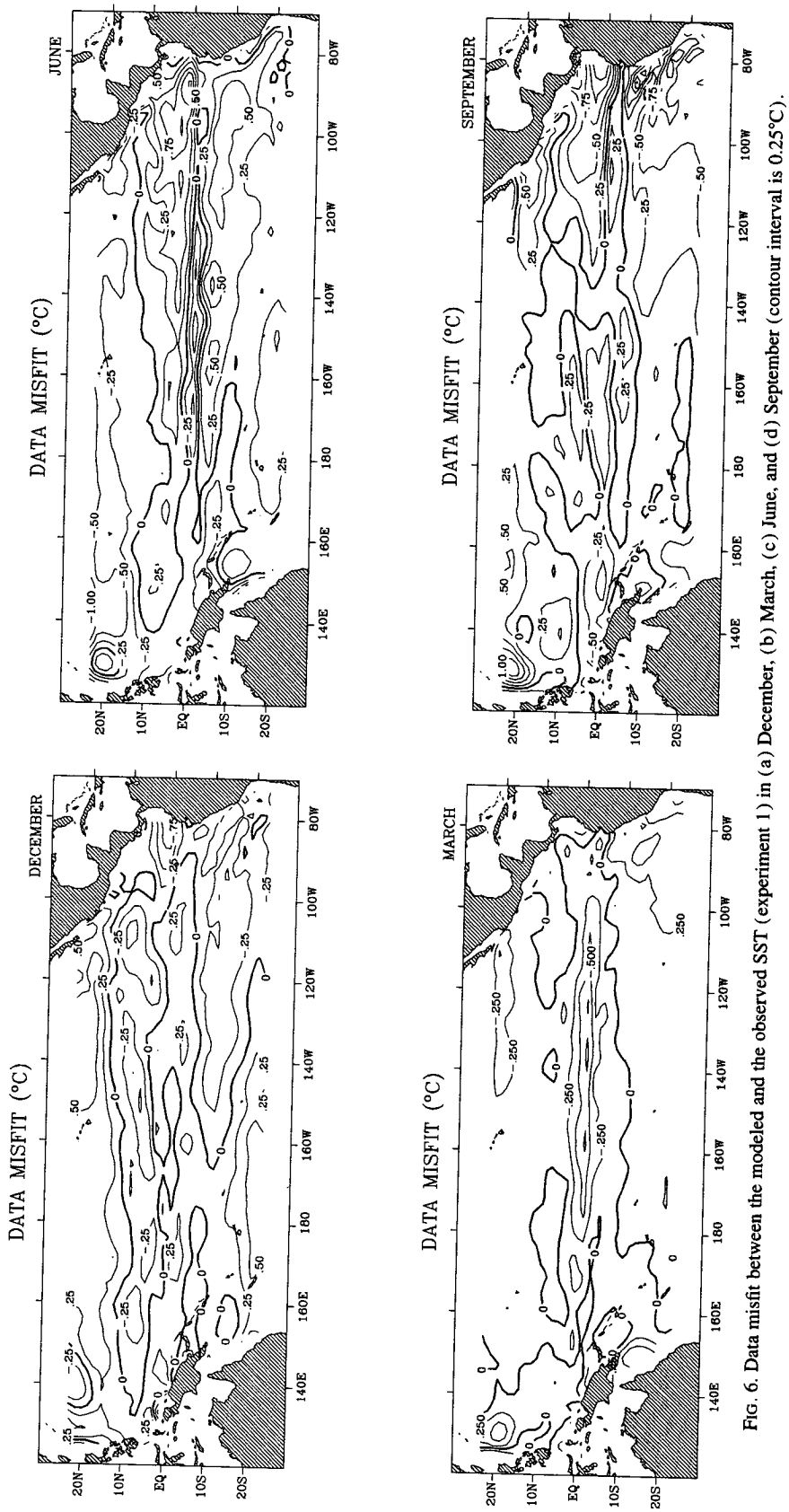

FIG. 6. Data misfit between the modeled and the observed SST (experiment 1) in (a) December, (b) March, (c) June, and (d) September (contour interval is 0.25°C).

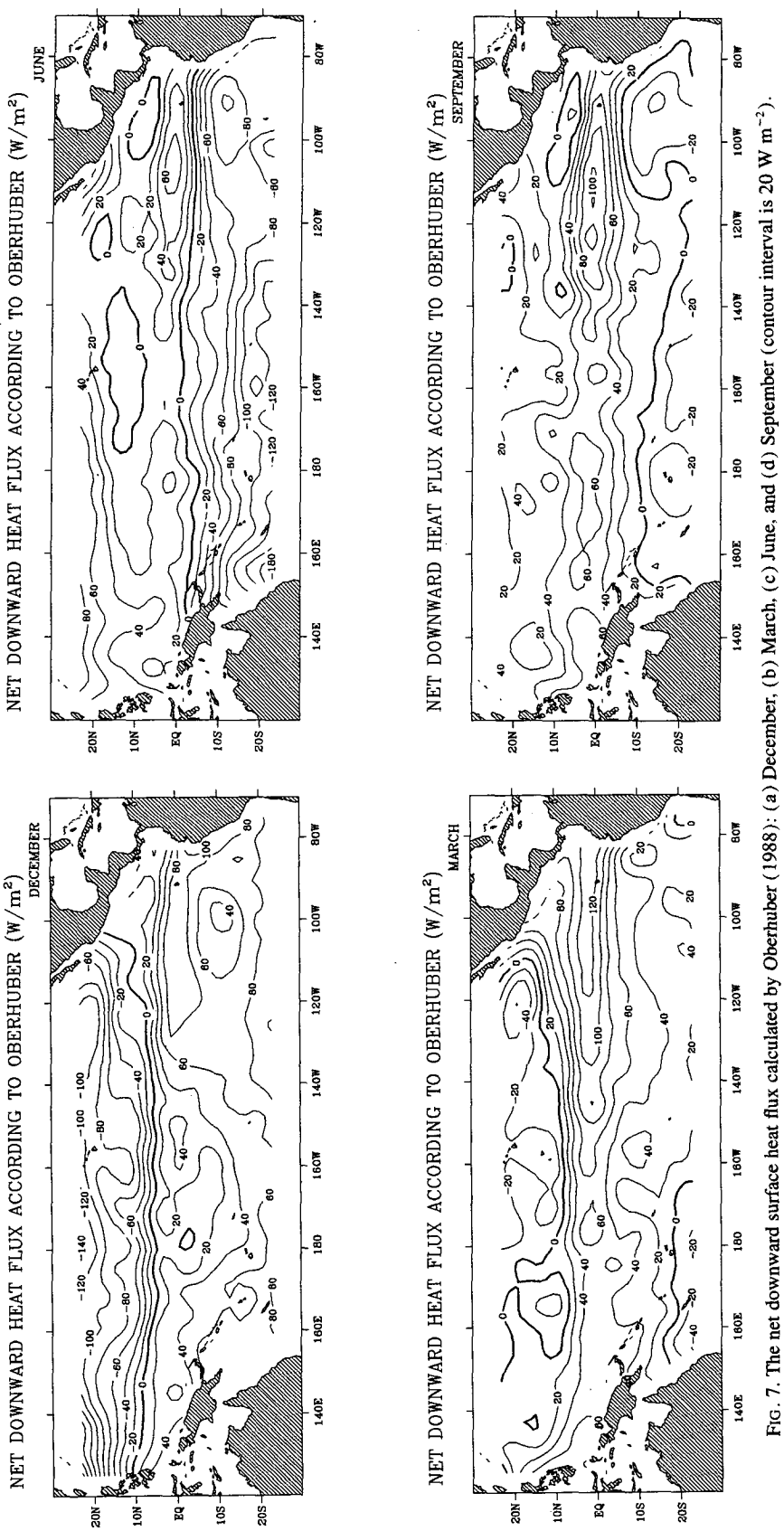

FIG. 7. The net downward surface heat flux calculated by Oberhuber (1988): (a) December, (b) March, (c) June, and (d) September (contour interval is 20 W m^{-2}).

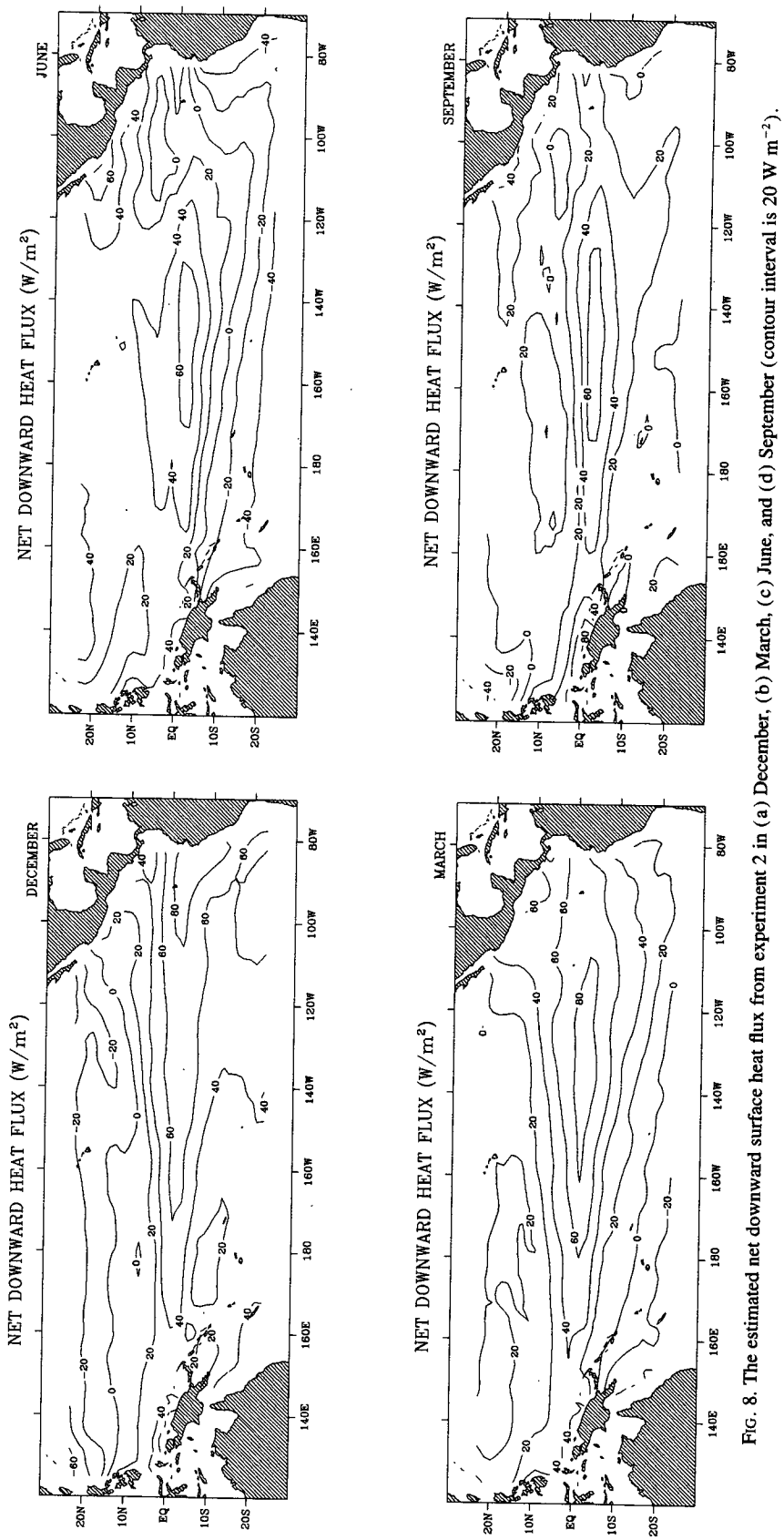

FIG. 8. The estimated net downward surface heat flux from experiment 2 in (a) December, (b) March, (c) June, and (d) September (contour interval is 20 W m^{-2}).

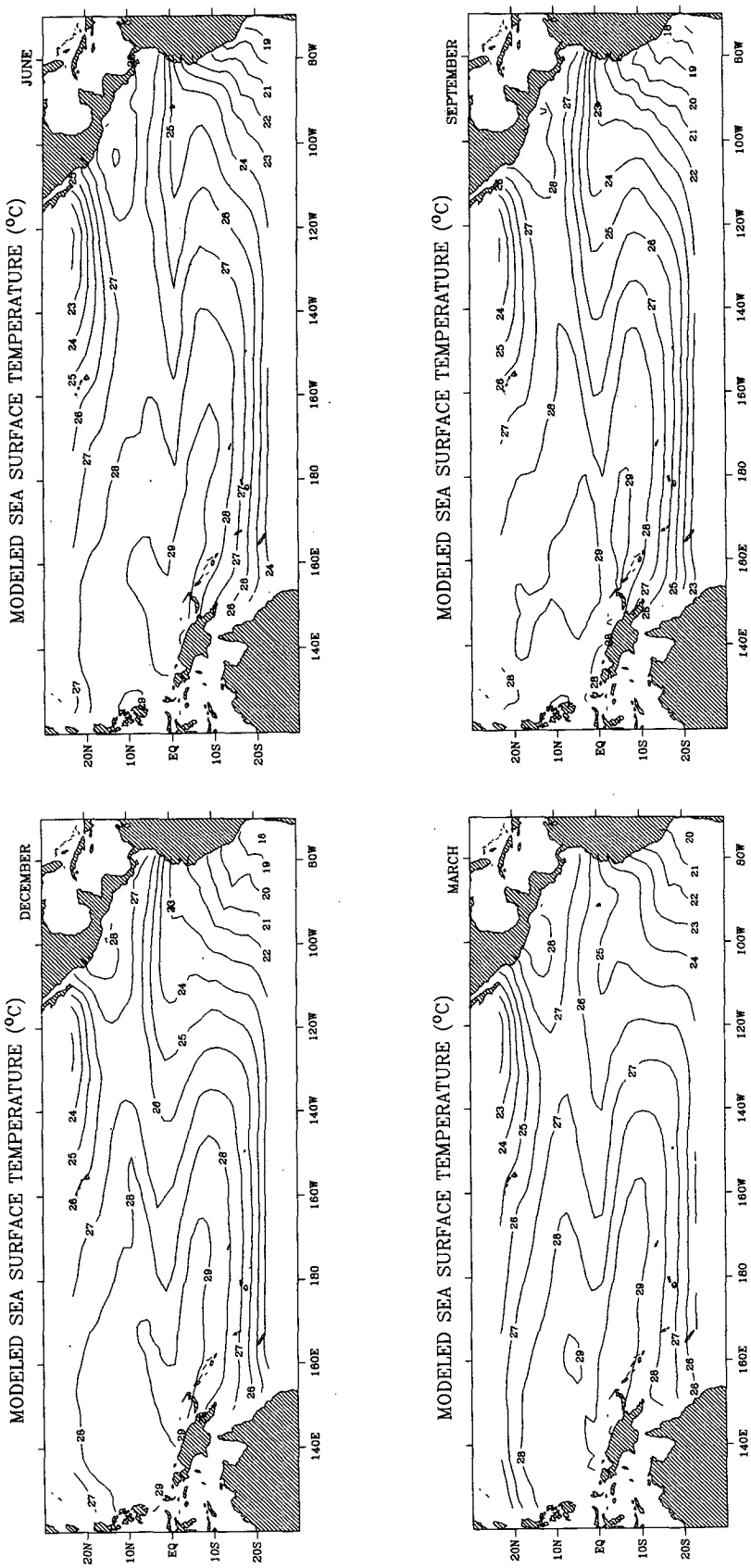

FIG. 9. The modeled sea surface temperature (SST) from experiment 2 in (a) December, (b) March, (c) June, and (d) September (contour interval is 1°C).

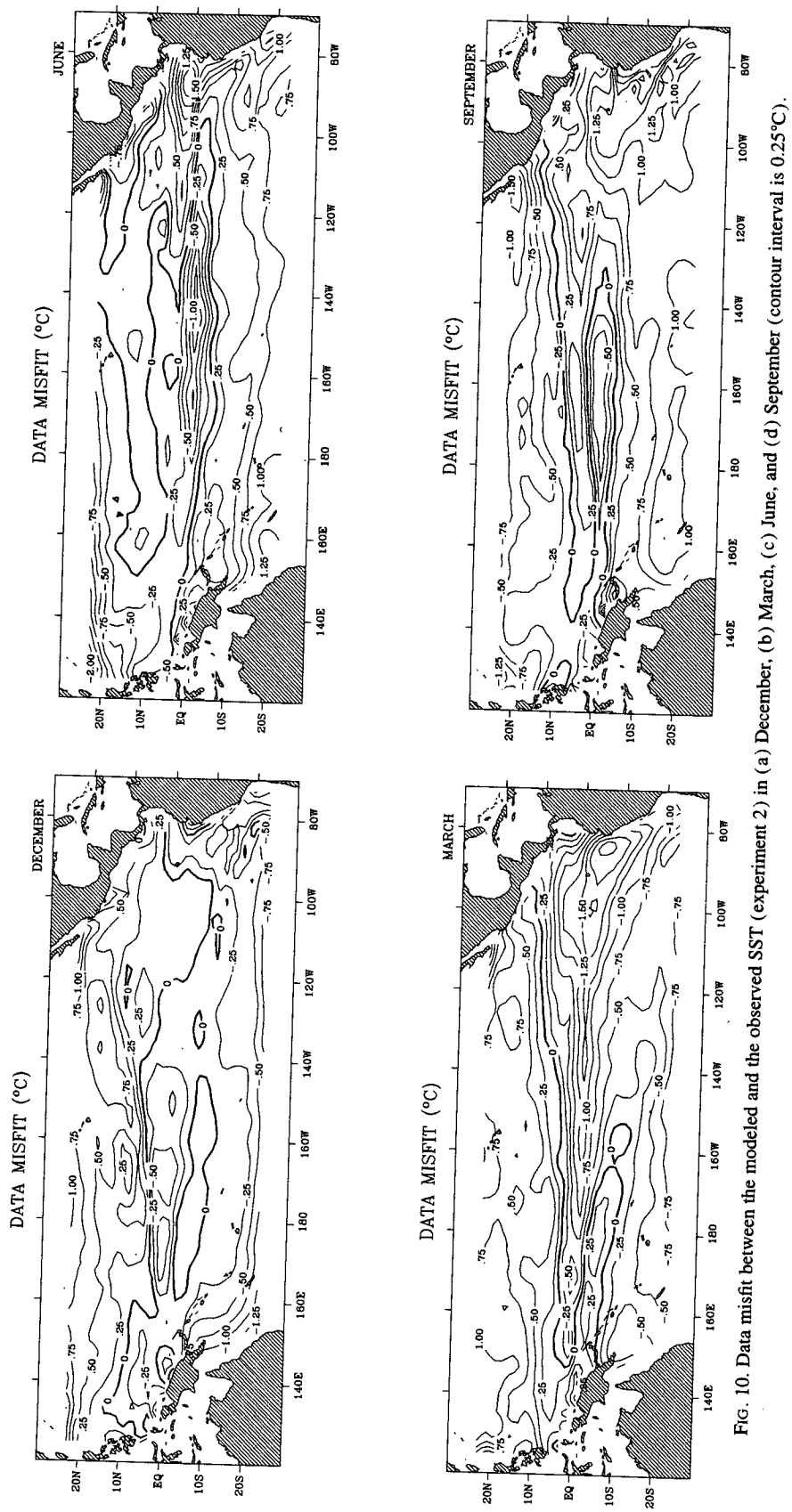

FIG. 10. Data misfit between the modeled and the observed SST (experiment 2) in (a) December, (b) March, (c) June, and (d) September (contour interval is 0.25°C).

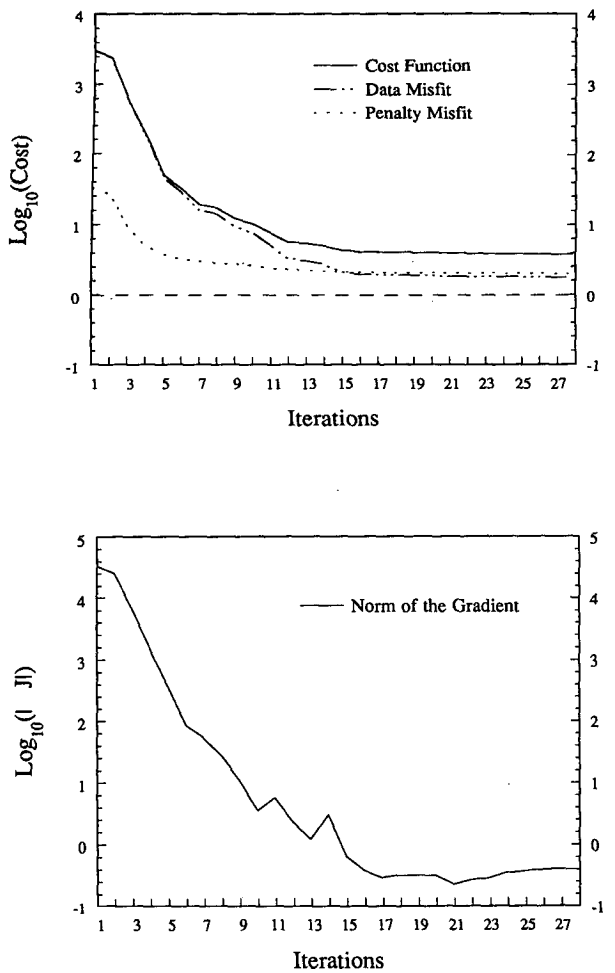

FIG. 11. The evolution of (a) the cost function (the zero line represents the standard deviation of the misfit) and (b) the norm of the gradient during the minimization (experiment 2).

The data used to produce the heat flux maps of O88 (Figs. 7a–d) and F90 (Figs. 13a–d) are the same COADS (Comprehensive Ocean–Atmosphere Dataset) described by Woodruff et al. (1987). The 30-year-average data (over the period of 1950–1979) are projected onto 2° × 2° grids in O88 and 4° × 4° grids in F90. Even though the data source is exactly the same, the two flux maps are different both quantitatively and qualitatively.

Examining Figs. 4, 7, and 13, one can observe that all of the three maps reveal similar seasonal variability, that is, seasonal alterations of the heat loss/gain outside of the equatorial zone and seasonal variations in the location and the strength of the heat flux maximum center in the eastern Pacific along the equator. The three maps also show that the variation of the heat flux is small year-round in the western Pacific warm pool area. The major difference among these maps is in the actual values associated with the maximum heat loss/gain centers.

The position of the zero flux line, in December, is almost identical in these three maps. The major difference arises in the eastern Pacific to the north of the equator where a strong heating center, over 120 W m^{-2}, exists in F90 (Fig. 5a), while it is absent in both O88 (Fig. 7a) and our map (Fig. 4a). Another difference occurs over the Kuroshio region where it seems that our procedure is inadequate in simulating the strength of the heat flux.

In March all three maps show a significant reduction of heat loss. The heat budget is near zero over a broad area of the northern Pacific. The major difference between our pattern (Fig. 4b) and either O88 (Fig. 7b) or F90 (Fig. 13b) is in the strength and location of the maximum heat gain in the eastern Pacific along the equator. The heat gain center, stretching westward from the coast of South America, forms a belt along the equator with the maximum value about 120 W m^{-2} in O88 and 160 W m^{-2} in F90. Our map shows that this equatorial heating maximum center moves offshore to about 120°W and has a slight reduction in strength compared to its own pattern in December.

In June the common features shown in all maps are the heat gain in the northern ocean, the strong heat loss in the southern ocean, and the intensive heating in the northeast along the coast of Mexico. The position of the zero flux line has almost the same latitudinal location in the central and western Pacific in all three maps but differs in the eastern Pacific. The heat gain center in our map is located at 140°W with a maximum value of 80 W m^{-2} (Fig. 4c), while both atlases show the location of the center at 105°W with 120 W m^{-2} in F90 (Fig. 7c) and 60 W m^{-2} in O88 (Fig. 13c). The intensive heat loss occurs along the coast of South America in our map but is away from the coast in both atlases.

In September the heat loss in the southern ocean has disappeared in our map (Fig. 4d) but is still visible in the atlases (Figs. 7d and 13d). In our map the heat gain belt moves slightly westward and spreads wider along the equator. The heat loss off the coast of South America is greatly reduced. O88 and F90 illustrate a similar feature in the variation of the heat gain center. For regions outside the equator a reverse heating pattern to that of springtime is observed in all of the three maps.

To summarize, the seasonal variations of the heat flux pattern from our adjoint calculations agree with those of O88 and F90 outside the equatorial zone except that the strength is weaker. F90 gives the maximum value throughout the climatology year. Our calculations fail in simulating the strong heat flux variability over the Kuroshio region in the northern wintertime. Inside the equatorial zone, the center of the maximum heat gain in our map has a different evolution in both location and strength from those of O88 and F90 in the eastern Pacific especially along the coast of South America.

The net heat flux is determined by the heat exchange process between the sea surface and lower atmosphere.

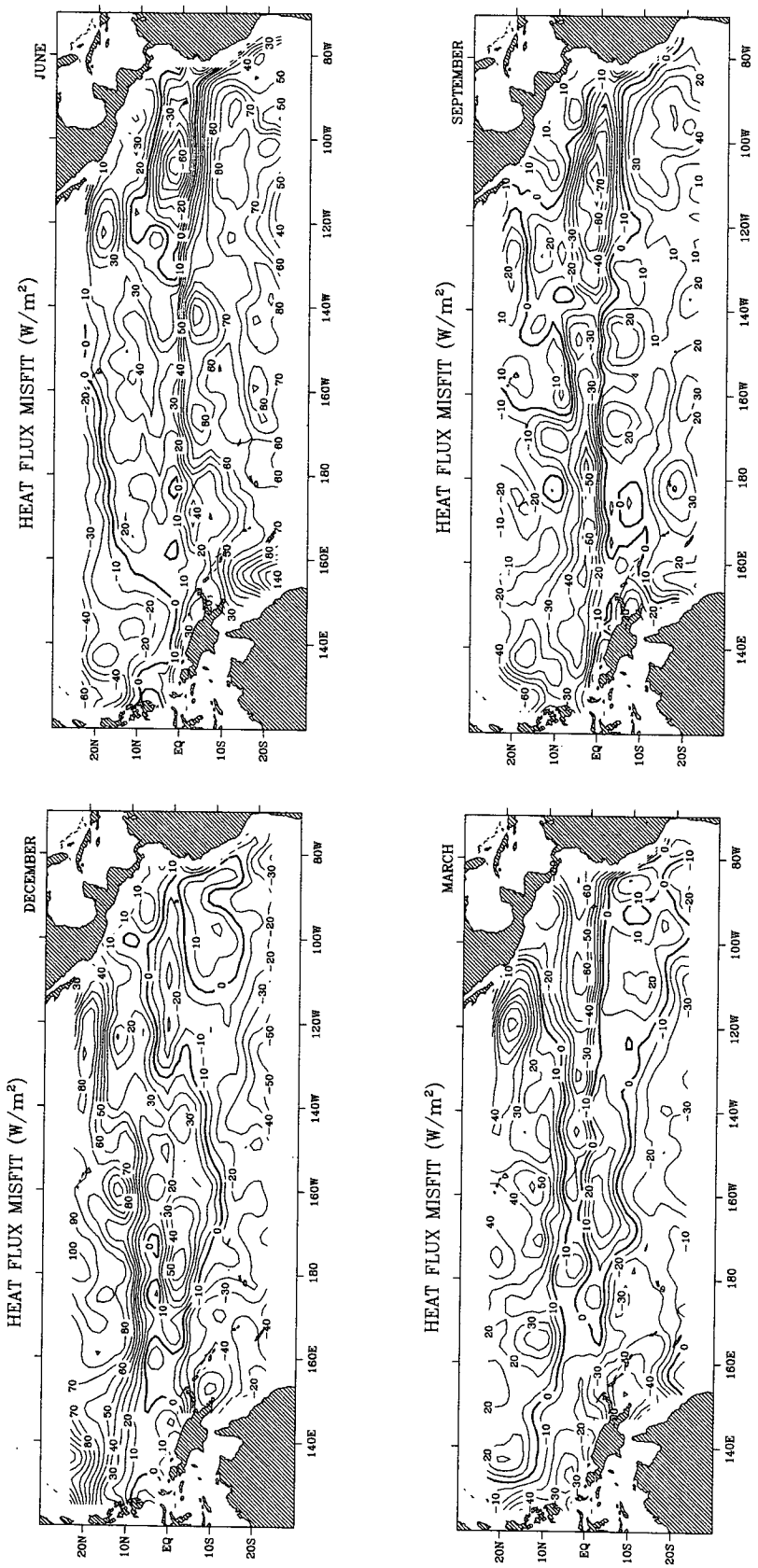

FIG. 12. Penalty misfit between the estimated heat flux and the Oberhuber heat flux in the experiment 2: (a) December, (b) March, (c) June, and (d) September (contour interval is 10 W m^{-2}).

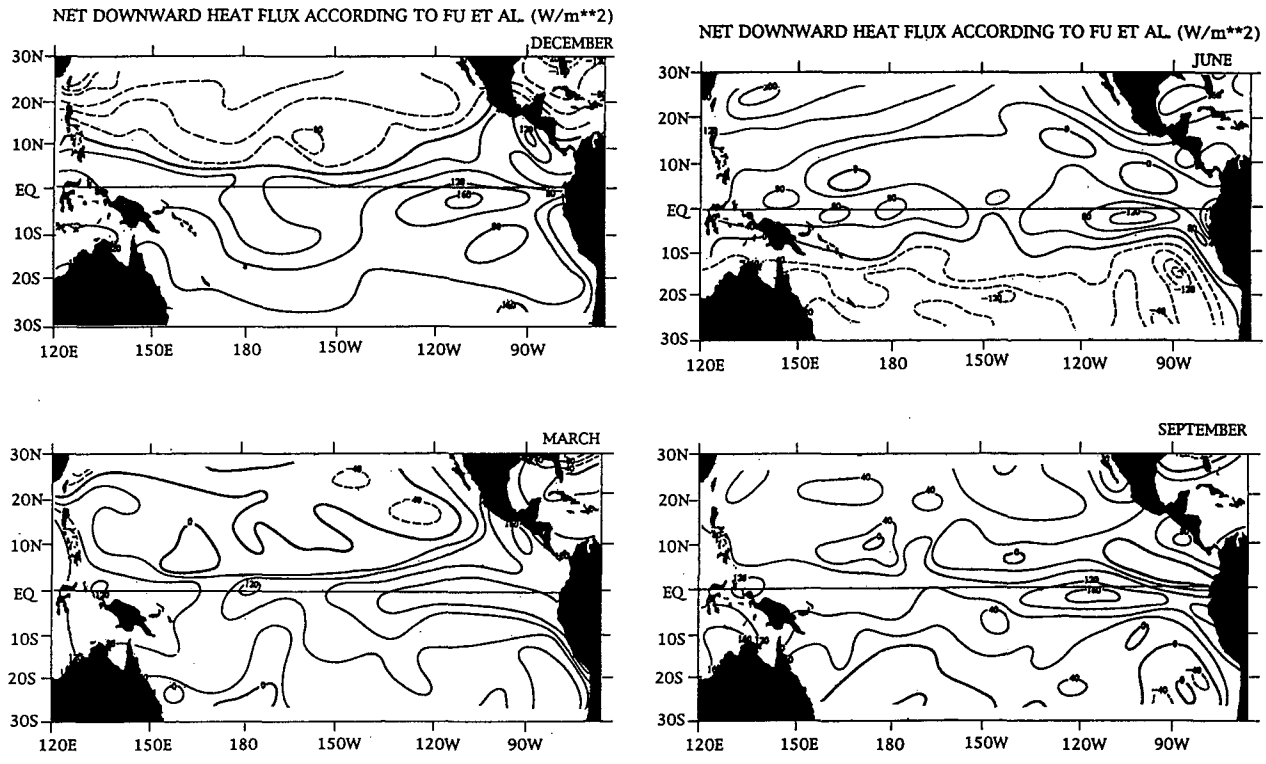

FIG. 13. The net downward surface heat flux from the atlas of Fu et al. (1990): (a) December, (b) March, (c) June, and (d) September (contour interval is 40 W m^{-2}).

In the next section we present the air–sea interaction mechanisms controlling the distribution of heat fluxes and study the thermodynamic relation between SST and surface heat flux from the SST equation. The divergence of our result from those atlases (O88 and F90), which used the bulk aerodynamic formulae, is discussed.

b. *Physical processes determining the heat flux distribution*

Of all components in the downward heat budget balance the solar radiation and latent heat flux are major contributors for surface heat flux variability. The loss of heat due to sensible heat flux is much less than the latent heat flux (about one-tenth).

The seasonal cycle of solar radiative flux is mainly defined by the change in albedo and is modified by seasonal variations of the cloud cover (see the atlases by Esbensen and Kushnir 1981; O88, F90). The solar heating varies primarily with latitude, decreasing from the equator to polar regions. The boreal ocean receives maximum solar incoming radiation from spring to summer, whereas the austral ocean has the minimum solar heating during this period.

The latent (sensible) heat fluxes are controlled by wind speed and the vertical gradient of humidity (temperature) at the ocean surface (e.g., Large and Pond 1982). The latent and sensible fluxes are varied seasonally outside the equatorial region. For the Northern Hemisphere they reach their maxima during autumn/winter due to the seasonal enhancement of the northeast trade winds and the large thermal or vapor difference near the ocean surface. The pattern reverses for the Southern Hemisphere. Within the equatorial region there is a low latent heat belt stretching along the equator with the minimum located near the coast of South America (e.g., O88 and F90).

The resulting net surface heat flux has a corresponding variation in seasonal timescales. During boreal autumn and winter the latent and sensible heat loss to the atmosphere over the northern ocean (southern ocean) is much larger (smaller) than the net solar radiation accumulated at the surface and therefore the ocean releases (gains) heat to (from) the atmosphere. For the rest of the year the northern (southern) ocean gains (loses) heat mainly due to the seasonal increase (decrease) of the solar incoming flux. The existence of the maximum heat flux in the eastern Pacific cold tongue region is the result of the minimal latent heat loss in this area.

Comparisons with the existing atlases show that the seasonal variation of the heat flux distribution from the adjoint calculations is consistent with that of the atlases. This proves that the adjoint procedure is a feasible method to study the flux variability.

c. Seasonal variations of the SST

Our net surface heat flux pattern is derived from the SST observations. Detailed examination of the SST seasonality will help us to understand the heat flux pattern obtained from the adjoint calculations and to explain the difference between the optimal flux map and the existing atlases. As is well documented in the oceanographic literature, there are three prominent SST centers in the tropical Pacific, namely, the warm SST center in the west-central Pacific (termed the warm pool), the cold SST center in the southeast Pacific (known as the cold tongue), and a warm SST center in the eastern Pacific to the north of the equator (Figs. 2a–d). The strong contrast between the warm pool in the west and the cold tongue in the east produces a remarkable SST horizontal gradient in the equatorial region. The SST isotherms are zonally oriented outside of the equatorial region.

Seasonal variability of the SST in the tropical Pacific is characterized by change of the warm pool and the cold tongue in their location and intensity. The seasonality is a combined result of several physical processes among which the solar insolation, latent heat release, upwelling and advection play the dominant role. The sensible heat exchange and longwave radiation from the sea surface are also important but their effects are one order smaller than that of the latent heat flux.

The net downward radiative flux (solar heating) is the main heating source for the ocean. It is directly responsible for SST seasonality away from the equator. For example, the SST in the North Pacific warms as the solar heating increases during boreal spring/summer. The warm pool (e.g., the 29° isotherm) moves northward as the center of insolation maximum shifts poleward. Meanwhile the South Pacific cools because of the austral winter there.

The existence of the equatorial SST minimum, however, cannot be explained by either solar heating or latent heat flux. A cold sea surface releases less heat to the atmosphere and the effect of the anomalous latent heat flux is to diminish the cooling in the cold tongue rather than to enhance it. In fact, the seasonal variability of the equatorial SST is related to the wind-driven upwelling and its effect on the thermocline depth (Wyrtki 1981).

The equatorial upwelling is a coupled dynamic–thermodynamic process. The easterly wind-driven Ekman divergence at the equator is balanced by an upward mass flux from the thermocline and thus cold water is brought to the surface. The prevailing easterly trade winds over the tropical Pacific cause the sea surface to slope up toward the west. This results in a deeper thermocline in the west than in the east and produces the east–west variations in upwelling intensity. Because of the shallower thermocline in the east, more rapid cooling can be produced by the turbulent mixing. From the above analysis one can see that variability of the SST in the tropical Pacific is determined by both surface heat flux and advection processes.

The optimal SST field obtained from the adjoint calculations (Figs. 5a–d) shows that the modeled SST field well resembles the observational SST outside of the equatorial region. In the equatorial region seasonal variations of the cold tongue in both model and observations follow the same cycle; that is, the cold tongue is weakest in the Northern Hemisphere spring and strongest in autumn. However, the shape of the modeled cold tongue is somewhat different from that of observations. There is a more westward extension of the cold tongue in the model than in observations.

d. Why is there a difference between the adjoint-calculated heat flux and the atlases over the region of the cold tongue?

Comparisons in section 4b(1) have shown that the evolution of the heat flux over the cold tongue from the adjoint calculations is different from that of the atlases in both location and strength, in particular during boreal summer. Therefore, one could ask, Is the adjoint-calculated heat flux pattern reasonable?

In the southeast Pacific along the South American coast the SST decreases by about 4°–5°C during northern summer (Figs. 2c,d). Two mechanisms can be traceable for the appearance of this cooler SST: One is the cooling induced by upwelling and the other is cooling due to surface heat loss. Although the upwelling pattern shows that the coastal upwelling is more intensified in summer than in spring (Figs. 14b–c), its strength in summer is much weaker than the equatorial upwelling. Therefore the rapid SST decreases must be caused by the other cooling mechanism, that is, the surface heat release. It is no surprise to observe the large amount of heat loss (over 120 W m^{-2}) along the coast of the South America in our heat flux map of June (Fig. 4c). This feature is missing in both O88 and F90.

From the analysis of the air–sea interactions during this period we can see that this large heat release is reasonable. Off the coast of South America, the northern summer is the time of year that the amount of cloud cover is at its maximum and hence incoming solar heating is at a minimum (see F90). This is also the season that southeast trade winds are intensified and, thus, latent heat release is increased (see F90). Both mechanisms have the effect of reducing the net downward heat flux and contribute to the appearance of the large negative heat flux. Therefore, the large amount of heat loss over the cold tongue region is essential for the significant SST reduction. The heat flux pattern from the adjoint calculations well represents the air–sea heat transport during summertime.

e. Data misfit

The data misfit pictures (Figs. 6a–d) have displayed a systematic larger discrepancies occurring in the

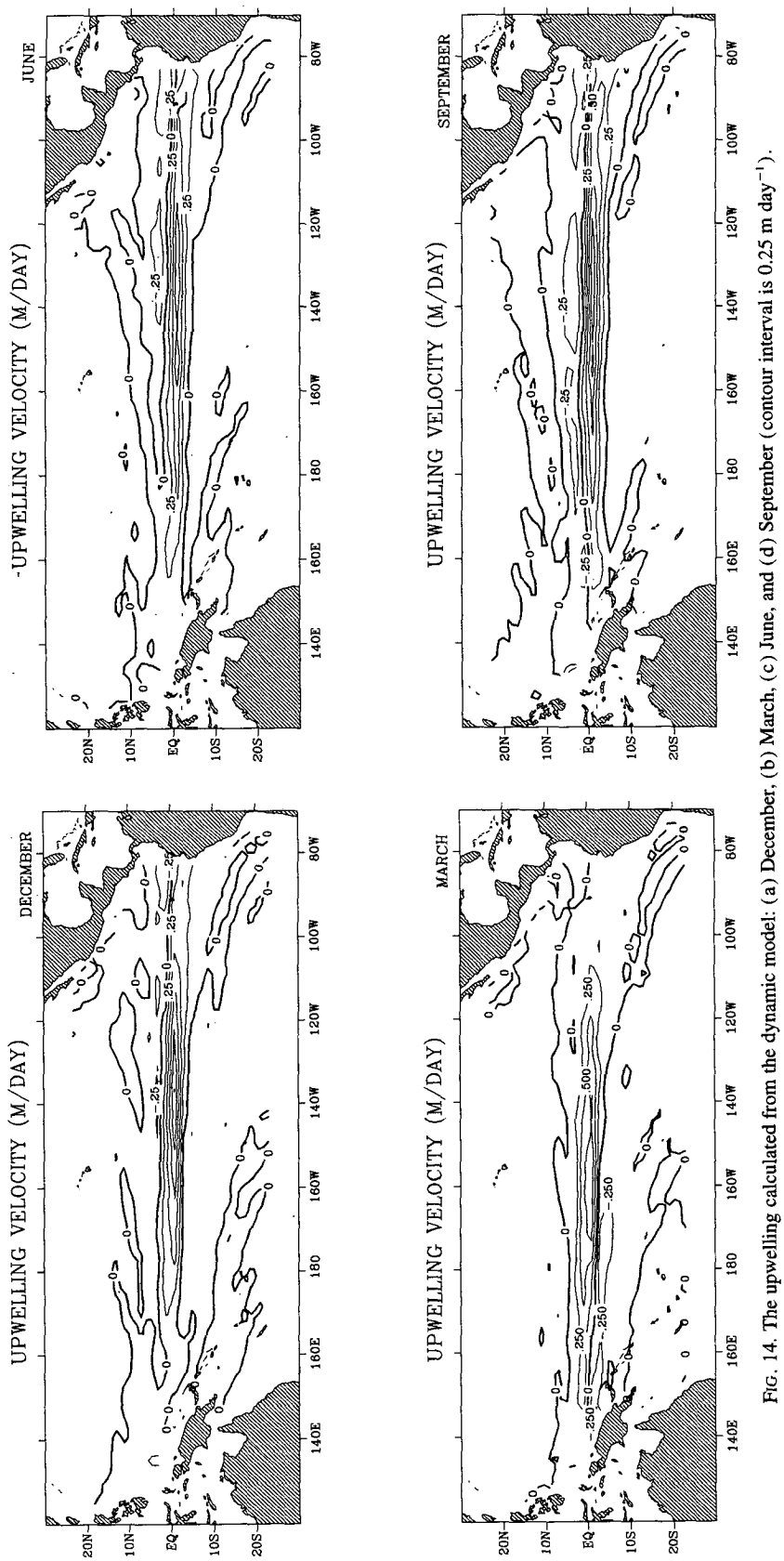

FIG. 14. The upwelling calculated from the dynamic model: (a) December, (b) March, (c) June, and (d) September (contour interval is 0.25 m day^{-1}).

regions associated with the cold tongue and the Kuroshio. This scenario seems contradictory to what has been assumed when using the diagonal weighting matrix. When formulating the cost function (2.7), we have made an assumption that the errors in the data are uncorrelated and equally weighted; therefore, the weighting matrix $\mathbf{K}_T$ is reduced to a unit matrix multiplied by a constant [see (2.6)]. Therefore, we anticipate a noisy and random misfit pattern rather than the systematic one. We believe that the appearance of the larger misfit in the cold tongue and the Kuroshio is attributable to the model's shortcomings. The major deficiency of the model is the adoption of a constant surface layer in resolving the physics of the near-surface region, which may not be practical in representing the intensity of the upwelling.

By choosing the surface layer depth to be 50 m the temperature of the entrained water (T_d) is represented by the temperature at 50-m depth (T_{50}) and is parameterized in terms of the vertical displacement of the model thermocline in the same way as Seager et al. (1988). By doing so, the intensity of the upwelling is strongly dependent on the temperature at 50 m. For a deep thermocline (e.g., the western equatorial Pacific) the upwelled water from above the thermocline is warm. For a shallow thermocline (e.g., the eastern equatorial Pacific) the upwelled water from the thermocline region is cold. Such formulation may not well represent the seasonal change of the upwelling strength in the cold tongue. It might give a stronger upwelling and produce cooler surface water in this area during the northern spring. This might be the reason for the appearance of the negative data misfit in Figs. 6a,b. While during the northern summer and autumn the upwelling there is much intensified due to the increased southeast trade wind. Observations (e.g., Fielder 1992) have shown that isotherms can outcrop at the surface and water can be upwelled from a much deeper depth. However, the model formulation excludes the physics associated with isotherm outcropping, and is unable to simulate the strength of upwelling during this period. It is then not surprising to observe the warmer model SST in the eastern Pacific during this period (Figs. 5c–d).

The model is essentially formulated to simulate the dynamics of the equatorial ocean only. The parameterization of entrainment is so simple that it may not be applicable to regions outside the equatorial zone. We conjecture that the larger data misfit in the northwestern Pacific, that is, the Kuroshio region, may be partly due to the lack of midlatitude dynamics in the model and/or the open boundary condition with the western boundary current and/or the low horizontal resolution (2°long by 2°lat), which makes it impossible to maintain the strength of the very narrow western boundary current.

Therefore, the greater departure of the modeled SST from the observed SST in the regions of the cold tongue and the Kuroshio might indicate that the model formulation for these regions needs to be improved; certainly a better result can be expected if a more sophisticated model is employed.

5. Summary and conclusions

A tropical oceanic model with thermodynamics is used to determine the surface thermal forcing field by the variational adjoint technique. Two datasets are chosen: the climatological monthly mean SST and surface winds. However, the underlying assumption of the model formulation enables us to decouple the model dynamics from the thermodynamics, and therefore only the SST data enter the assimilation procedure.

We have performed two experiments to examine the optimal solution obtained under different approaches. Experiment 1 adopts an approach that takes into consideration the uncertainty in the weights and requires the procedure to determine the optimal weights, while experiment 2 borrows the commonly used adjoint approach in which the weights are prescribed before conducting the assimilating process. The scheme in experiment 1 asks the prior information $\tilde{Q}$ to represent the smoothness character of the solution, while experiment 2 takes observations as the prior information. The expectations in these two schemes are incommensurate so that the two solutions are fundamentally not comparable, though both approaches fall into the same theoretical framework (2.5). We would also like to point out that in experiment 1 the impact of the prior information on the final solution is not readily quantifiable. Rigorous understanding of the properties of this scheme await future work.

The results illustrate that the model, although simple, is capable of determining seasonal variations of the surface heat flux by assimilating the SST observations. By comparing the heat flux pattern from experiment 1 with the existing heat flux atlases of Oberhuber (1988) and Fu et al. (1990) one can see that our adjoint procedure has successfully captured the seasonal signals of the surface heat flux distribution over the tropical Pacific Ocean. The analysis of the physics of the air–sea interaction indicates that the adjoint method is a practical way to infer the heat flux information from the available SST data.

The data misfits between the modeled and observed SST reveal that the model agrees well with SST observations within the estimation of the observation accuracy of 1°C. The only exceptions are in the areas of the cold tongue and the Kuroshio where a departure greater than 1°C appears. We conjecture that this larger misfit is the result of the model's shortcomings. The formulation of the model includes a constant surface layer, which may not well represent the strength of upwelling at the equator and along the coast. The model formulation also focuses on the simulation of equatorial dynamics; therefore it may lack the midlatitude physics in resolving the features related to the Kuroshio.

The results from this research are very promising. It provides a way for extracting the surface heat flux information directly from SST data. In addition, it ensures that the estimated heat flux pattern is consistent with the model intrinsic physics. This in turn allows us to be able to explain the calculated model fields in terms of the model physics and to discover the weakness of the model formulation by comparison with data.

The methodology used here can be easily extended to determine the surface wind forcing field. As many applications have proved, the adjoint method is so versatile and powerful that it can be used to adjust any model parameters as long as there are sufficient observations available.

Acknowledgments. We are grateful to Michael Navon for his valuable comments and expert help. The two anonymous reviewers are greatly appreciated for their thorough reviews and for their critical comments. The Supercomputer Computations Research Institute (SCRI) at Florida State University is acknowledged for their support to L. Yu during a portion of this work. Our research in ocean data assimilation is sponsored by NASA, Ocean Processes. The base support for COAPS comes from the Secretary of Navy Grant to JJO.

REFERENCES

Anderson, D. L. T., 1991: Data assimilation in ocean models. *Strategies for Future Climate Research,* M. Latif, Ed., Max-Plank-Institut für Meteorologie, 193–225.

Bard, Y., 1974: *Nonlinear Parameter Estimation.* Academic Press, 340 pp.

Bennett, A. F., 1992: *Inverse Methods in Physical Oceanography.* Cambridge University Press, 346 pp.

Blanc, T. V., 1987: Accuracy of bulk-method-determined flux, stability, and sea surface roughness. *J. Geophys. Res.,* **92,** 3864–3876.

Bussalacchi, A. J., and J. J. O'Brien, 1980: The seasonal variability in a model of the tropical Pacific. *J. Phys. Oceanogr.,* **10,** 1929–1951.

Camerlengo, A. L., and J. J. O'Brien, 1980: Open boundary conditions in rotating fluids. *J. Comput. Phys.,* **35,** 12–35.

Cane, M. A., 1979: The response of an equatorial ocean to simple wind stress patterns: Part I. Model formulation and analytical results. *J. Mar. Res.,* **37,** 233–252.

Carrera, J., and S. P. Neuman, 1986a: Estimation of aquifer parameters under transient and steady state conditions. 1: Maximum likelihood method incorporating prior information. *Water Resour. Res.,* **22**(2), 199–210.

——, and ——, 1986b: Estimation of aquifer parameters under transient and steady state conditions. 2: Uniqueness, stability and solution algorithm. *Water Resour. Res.,* **22**(2), 211–227.

Cooley, R. L., 1977: A method of estimating parameters and assessing reliability for models of steady state groundwater flow. 1: Theory and numerical properties. *Water Resour. Res.,* **13**(2), 318–324.

——, 1982: Incorporation of prior information on parameters into nonlinear regression groundwater flow models. 1: Theory. *Water Resour. Res.,* **18**(4), 965–976.

Derber, J., 1987: Variational four-dimensional analysis using quasi-geostrophic constraints. *Mon. Wea. Rev.,* **115,** 998–1008.

Draper, N. R., and H. Smith, 1981: *Applied Regression Analysis.* John Wiley & Sons, 709 pp.

Esbensen, S. K., and Y. Kushnir, 1981: The heat budget of the global ocean: An atlas based on estimates from surface marine observations. Climate Research Institute, Oregon State University, Report No. 29, 133 pp.

Fielder, P. C., 1992: Seasonal climatologies and variability of eastern tropical Pacific surface waters. NOAA Tech. Rep. NMFS 109, 65 pp.

Fletcher, R., 1987: *Practical Methods of Optimization.* John Wiley & Sons, 436 pp.

Fu, C., M. Zhang, J. Fletcher, B. Su, and X. Quan, 1990: *Atlas of Climate Physics of Tropical Pacific Ocean.* Science Press, 190 pp.

Ghil, M., and P. Malanotte-Rizzoli, 1991: Data assimilation in meteorology and oceanography. *Advances in Geophysics,* Vol. 33, Academic Press, 141–266.

Large, W. G., and S. Pond, 1982: Sensible and latent heat flux measurements over the ocean. *J. Phys. Oceanogr.,* **12,** 464–482.

Le Dimet, F., and O. Talagrand, 1986: Variational algorithms for analysis and assimilation of meteorological observations: Theoretical aspects. *Tellus,* **38A,** 97–110.

Lewis, J. M., and J. C. Derber, 1985: The use of adjoint equations to solve a variational adjustment problem with advective constraints. *Tellus,* **37A,** 309–322.

Lions, J. L., 1971: *Optimal Control of Systems Governed by Partial Differential Equations.* Springer-Verlag, 369 pp.

Lorenc, A., 1986: Analysis methods for numerical weather prediction. *Quart. J. Roy. Meteor. Soc.,* **112,** 1177–1194.

Marotzke, J., and C. Wunsch, 1993: Finding the steady state of a general circulation model through data assimilation: Application to the North Atlantic ocean. *J. Geophys. Res.,* **98,** 20 149–20 167.

Moore, D. W., and S. G. H. Philander, 1978: Modeling of the tropical oceanic circulation. *The Sea,* Vol. 6, Goldberg et al., Eds., Wiley, 319–361.

Navon, I. M., and D. Legler, 1987: Conjugate-gradient methods for large-scale minimization in meteorology. *Mon. Wea. Rev.,* **115,** 1479–1502.

Neuman, 1973: Calibration of distributed parameter groundwater flow models viewed as a multiple-objective decision process under uncertainty. *Water Resour. Res.,* **9**(4), 1006–1021.

——, 1980: A statistical approach to the inverse problem of aquifer hydrology. 3: Improved solution method and added perspective. *Water Resour. Res.,* **16**(2), 331–346.

——, and S. Yakowitz, 1979: A statistical approach to the inverse problem of aquifer hydrology. 1: Theory. *Water Resour. Res.,* **15**(4), 845–860.

Oberhuber, J. M., 1988: An atlas based on the COADS data set: The budgets of heat, buoyancy and turbulent kinetic energy at the surface of the global ocean. Max-Plank-Institut für Meteorologie, 100 pp.

O'Brien, J. J., 1986: The diffusive problem. *Advanced Physical Oceanographic Numerical Modeling,* J. J. O'Brien, Ed., D. Reidel, 127–144.

Philander, S. G. H., and A. D. Siegel, 1985: Simulation of El Niño of 1982–1983. *Proc. 16th Int. Liege Colloq. on Ocean Hydrodynamics,* J. Nihoul, Ed., Elsevier Oceanogr. Ser., 517–541.

Seager, R., S. E. Zebiak, and M. A. Cane, 1988: A model of the tropical Pacific sea surface temperature climatology. *J. Geophys. Res.,* **93,** 1265–1280.

Shanno, D. F., and K. H. Phua, 1980: Remark on algorithm 500—A variable method subroutine for unconstrained nonlinear minimization. *ACM Trans. Math. Software,* **6,** 618–622.

Shea, D. J., K. E. Trenberth, and R. W. Reynolds, 1990: A global monthly sea surface temperature climatology. NCAR Tech. Note NCAR/TN-345+STR, 167 pp.

Stricherz, J. N., J. J. O'Brien, and D. M. Legler, 1992: Atlas of Florida State University Tropical Pacific Winds for TOGA 1966–1985. A mesoscale Air–Sea Interaction Group Technique Report, The Florida State University, 216 pp.

Talagrand, O., and P. Courtier, 1987: Variational assimilation of meteorological observations with the adjoint vorticity equation. Part I: Theory. *Quart. J. Roy. Meteor. Soc.*, **113,** 1311–1328.

Thacker, W. C., 1988: Fitting models to data by enforcing spatial and temporal smoothness. *J. Geophys. Res.*, **93,** 10 655–10 665.

——, and R. B. Long, 1988: Fitting dynamics to data. *J. Geophys. Res.*, **93,** 1227–1240.

Tziperman, E., W. C. Thacker, R. B. Long, S. Huang, and S. R. Rintoul, 1992: Oceanic data analysis using a general circulation model. Part II: A North Atlantic model. *J. Phys. Oceanogr.*, **22,** 1458–1485.

Weare, B. C., P. T. Strub, and M. D. Samuel, 1981: Annual mean surface heat fluxes in the tropical Pacific ocean. *J. Phys. Oceanogr.*, **11,** 705–717.

Wunsch, C., 1989: Tracer inverse problems. *Oceanic Circulation Model: Combining Data and Dynamics.* D. L. T. Anderson and J. Willebrand, Eds., D. Reidel, 1–78.

Wyrtki, K., 1981: An estimate of equatorial upwelling in the Pacific. *J. Phys. Oceanogr.*, **11,** 1205–1214.

Yu, L., 1992: Determining the surface heat flux distribution over the tropical Pacific ocean by the adjoint method. Ph.D. dissertation, The Florida State University, 167 pp.

——, and J. J. O'Brien, 1991: Variational estimation of the wind stress drag coefficient and the oceanic eddy viscosity profile. *J. Phys. Oceanogr.*, **21,** 709–719.

——, and ——, 1992: On the initial condition in parameter estimation. *J. Phys. Oceanogr.*, **22,** 1361–1364.

Zebiak, S. E., and M. A. Cane, 1987: A model El Niño–Southern oscillation. *Mon. Wea. Rev.*, **115,** 2262–2278.